

1 **Lower-stage plane bed topography is an outcome of**
2 **rarefied, intermittent sediment transport**

3 **Thomas C. Ashley¹, Suleyman Naqshband², Brandon McElroy¹**

4 ¹Department of Geology and Geophysics, University of Wyoming, Laramie, WY

5 ²Department of Environmental Sciences, Wageningen University, Wageningen, Netherlands

6 **Key Points:**

- 7 • Experiments highlight differences in particle behavior over stable and unstable pla-
8 nar topography.
9 • Stable bed configuration is controlled by a critical transition in particle behavior
10 related to collisions between mobile particles.
11 • Predicted threshold of bedform initiation mirrors classic empirical stability dia-
12 grams.

Corresponding author: Thomas C. Ashley, tashley22@gmail.com

13 **Abstract**

14 Sedimentary bed configurations that are stable under weak fluid-driven transport
 15 conditions can be divided into two groups: (1) meso-scale features that influence flow
 16 and sediment transport through roughness and drag partitioning effects (“mesoforms”),
 17 and (2) grain-scale features that can effectively be ignored at the macroscopic scale (“mi-
 18 croforms”). In practice, these groups delineate ripples and dunes from quasi-planar bed
 19 configurations. They are thought to be separated by a transition in processes govern-
 20 ing the relief of the bed; however, the physical mechanisms responsible for this transi-
 21 tion are poorly understood. Previous studies suggest that planar topography is unsta-
 22 ble when interactions between moving particles lead to stabilized bed disturbances that
 23 initiate morphodynamic pattern coarsening. This study presents a kinetic interpretation
 24 of this hypothesis in terms of parameters describing particle motion. We find that the
 25 microform/mesoform transition corresponds to a critical transition in particle behavior
 26 associated with increasing importance of particle collisions. This transition also corre-
 27 sponds to the point where continuum-based morphodynamic models are permissible at
 28 the most unstable wavelength predicted from linear stability theory, providing a link be-
 29 tween descriptive and mathematical theories of bedform initiation.

30 **1 Introduction**

31 Self-organized bedforms like ripples and dunes are essential equilibrium features
 32 of fluid driven sediment transport. They influence macroscopic flow and sediment trans-
 33 port through roughness and drag partitioning effects (Einstein, 1950; Engelund & Hansen,
 34 1967; Smith & Mclean, 1977; Fredsoe, 1982; van Rijn, 1984; Wright & Parker, 2004; Best,
 35 2005) and produce cross-bedded sedimentary architecture that can be used to interpret
 36 past flow conditions (Paola & Borgman, 1991; Leclair & Bridge, 2001; Mahon & McEl-
 37 roy, 2018; Leary & Ganti, 2020). However, planar topography has been observed over
 38 a narrow range of bed stresses near the threshold of motion in sand and gravel (Figure
 39 1). Predicting the occurrence of planar topography is important from a practical stand-
 40 point because (a) grain roughness is the primary source of flow resistance (Engelund &
 41 Fredsoe, 1982), (b) sediment transport is efficient because energy is not lost to form drag
 42 (Wiberg & Smith, 1989), and (c) primary current stratification lacks recognizable cross-
 43 bedded structures (Leeder, 1980; Baas et al., 2016). Moreover, weak bedload transport
 44 conditions are common in rivers due to apparently universal constraints governing the
 45 geometry of self-formed channels (Lacey, 1930; Schumm, 1960; Ikeda et al., 1988; Dade
 46 & Friend, 1998; Eaton et al., 2004; Parker et al., 2007; Wilkerson & Parker, 2010; Métivier
 47 et al., 2017; Dunne & Jerolmack, 2018).

48 Despite this need, the mechanisms that control the stable bed configuration un-
 49 der weak bedload transport conditions are poorly understood. Studies focused on ob-
 50 servation and documentation of morphodynamic phenomena have produced valuable de-
 51 scriptive theories of bedform initiation, however these are often limited in terms of their
 52 predictive power (e.g., Langbein & Leopold, 1968; P. B. Williams & Kemp, 1971; Costello,
 53 1974; Leeder, 1980; Coleman & Melville, 1994; Coleman & Nikora, 2009). The primary
 54 theoretical approach to this problem involves modeling the fate of sinusoidal bed distur-
 55 bances subject to coupled equations describing flow, sediment transport and topogra-
 56 phy (e.g., Engelund & Fredsoe, 1982; McLean, 1990; Fourrière et al., 2010; Andreotti et
 57 al., 2010; Charru et al., 2013; Bohorquez et al., 2019). This approach has clarified how
 58 simplified physical models can explain a number of commonly observed bed configura-
 59 tions like dunes, upper-stage plane bed, and antidunes, but most formulations predict
 60 that planar topography is unstable near the threshold of motion. One notable exception
 61 is the formulation of Andreotti et al. (2010). Their model predicts that the most stable
 62 wavelength approaches infinity at a finite excess stress in aeolian environments (Charru
 63 et al., 2013), but it is unclear whether it can explain observations of planar topography

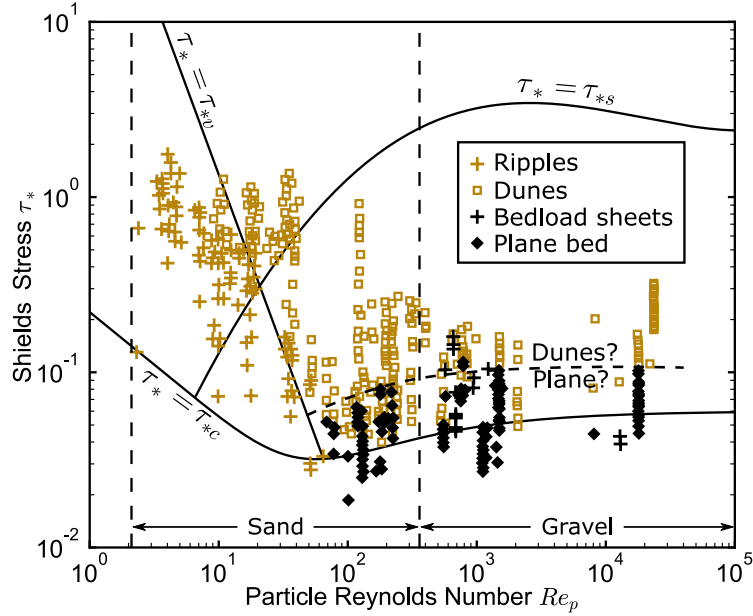


Figure 1. Shields-Parker river sedimentation diagram with empirical plane bed/dune threshold (dashed line) adapted from García (2008). The observations of bed configuration reported by Carling (1999) are plotted for comparison. Here, τ_{*v} is the viscous threshold Shields stress (García (2008), equation 2-78), τ_{*s} is the suspension threshold Shields stress (equation 2-75), and τ_{*c} is the critical Shields stress for sediment motion (equation 2-59a). Note that we distinguish between ripples and dunes according to their original classification (which may differ from modern criteria).

64 in rivers where the flow disturbance is expected to be transitional rather than fully tur-
 65 bulent.

66 In general, mathematical analyses have not led to a definitive explanation for the
 67 transition from stable to unstable planar topography observed in field and experimen-
 68 tal data (Figure 1). To understand why, we look to descriptions of flow and transport
 69 processes near the threshold of motion that have not been reconciled with modern
 70 stability theory. First, consider that a precise definition of lower-stage plane bed topog-
 71 raphy must recognize that the concept of a planar bed breaks down at scales approach-
 72 ing the diameters of grains. The random motion of particles driven by turbulent fluid
 73 flow causes disturbances in bed elevation (Leeder, 1980; Gyr & Schmid, 1989; Best, 1992)
 74 such that the minimum relief of a mobile bed undergoing active sediment transport is
 75 several times the nominal particle diameter (Whiting & Dietrich, 1990; Clifford et al.,
 76 1992). Notably, Martin et al. (2014) modeled evolution of grain-scale bed disturbances
 77 as a mean-reverting random walk, illustrating how a competition between disturbance
 78 growth and relaxation leads to a total bed relief that is proportional to particle diam-
 79 eter across a range of weak transport conditions.

80 Grain-scale bed disturbances may remain stable, or they may initiate pattern coarsen-
 81 ing through nonlinear feedbacks between flow, sediment transport and topography (hence-
 82 forth, “morphodynamic coarsening”). Previous studies observed the onset of significant
 83 flow separation behind disturbances (P. B. Williams & Kemp, 1971; Leeder, 1980; Best,
 84 1996; Gyr & Kinzelbach, 2004) and defect propagation through scour-deposition waves
 85 (Raudkivi, 1963, 1966; Southard & Dingler, 1971; Costello & Southard, 1981; Gyr & Schmid,
 86 1989; Best, 1992; Venditti et al., 2005a) when bed disturbances exceed a critical height

87 of 2-4 particle diameters (P. B. Williams & Kemp, 1971; Leeder, 1980; Costello & Southard,
 88 1981; Coleman & Nikora, 2009, 2011). Based on their own observations and an exten-
 89 sive review of previous work, Coleman and Nikora (2009) argued that bedform initia-
 90 tion is characterized by a two stage process. In the first stage, individual mobile parti-
 91 cles and clusters of particles interact and create grain-scale bed disturbances when they
 92 come to rest. The second stage begins when grain-scale bed disturbances become suf-
 93 ficiently large to interrupt the bedload layer. We suggest that this critical disturbance
 94 height defines a transition in process regime that suitably differentiates morphodynamically-
 95 scaled “mesoforms” (e.g., ripples and dunes) from microforms like bedload sheets, par-
 96 ticle clusters, and low-relief bedforms that scale primarily with particle diameter. Be-
 97 low this threshold, the bed configuration may be treated as quasi-planar for most prac-
 98 tical purposes because (a) mobile bed roughness models already include the effect of mi-
 99 croforms, (b) flow separation is poorly developed such that drag partitioning effects can
 100 be ignored for the purposes of predicting sediment load, and (c) preserved cross-bedding
 101 structures have a maximum thickness of several particle diameters and are likely to be
 102 indistinguishable from planar laminations in stratigraphy.

103 Based on this criterion, the question of bedform stability reduces to the problem
 104 of identifying the processes that control the height of grain-scale bed disturbances. De-
 105 scriptive studies often report qualitative differences in collective particle behavior over
 106 stable and unstable planar topography that appear to be related to disturbance growth
 107 (Bagnold, 1935; P. B. Williams & Kemp, 1971; Costello, 1974; Coleman & Nikora, 2011).
 108 Specifically, when planar topography is stable, transport is characterized by occasional,
 109 intermittent motions of individual sediment particles. In contrast, transport over unsta-
 110 ble planar topography is characterized by a marked increase in the overall mobility of
 111 the bed with many moving particles forming mobile patches, streaks, and hummocks (Southard
 112 & Dingler, 1971; Costello, 1974; Costello & Southard, 1981). These descriptions evoke
 113 transport thresholds that have been described in a variety of other contexts; for exam-
 114 ple, the transition from partial to full mobility observed in gravel bedded rivers (Wilcock
 115 & McArdell, 1997; Pfeiffer & Finnegan, 2018), and the transition from intermittent to
 116 continuous transport recognized in both field and numerical studies of granular motion
 117 (González et al., 2017; Martin & Kok, 2018; Pähtz et al., 2020). A number of authors
 118 also suggest that the growth of bed disturbances is connected to interactions between
 119 moving particles and congestion in the bedload phase (Bagnold, 1935; Langbein & Leopold,
 120 1968; Costello, 1974; Coleman & Melville, 1996; Coleman & Nikora, 2009).

121 Our primary hypothesis is that the transition from stable to unstable planar to-
 122 pography is driven by a critical transport threshold associated with an increase in the
 123 importance of mobile particle interactions (“collisions”). Topographic evolution occurs
 124 through the entrainment and disentrainment of individual sediment particles; thus, we
 125 suggest that the morphodynamic importance of particle collisions may be evaluated by
 126 comparing an estimate of the particle collision frequency Z_g ($L^{-2}T^{-1}$) (particle collision
 127 events per second per unit bed area) with the particle entrainment frequency E_g ($L^{-2}T^{-1}$)
 128 (particle entrainment events per second per unit bed area). The ratio $\theta = Z_g/E_g$ (hence-
 129 forth, the “collision number”), characterizes the potential for particle collisions to influ-
 130 ence topographic change and may be interpreted as the average number of collisions from
 131 entrainment to disentrainment. When $\theta < 1$, collisions are rare and transport is dom-
 132 inated by isolated motions of individual particles. When $\theta > 1$, the average particle hop
 133 involves at least one collision, promoting the formation of mobile clusters of particles.
 134 Thus, we hypothesize that there is a threshold value $\theta \approx 1$ that separates transport con-
 135 ditions where planar topography is stable from transport conditions where planar topog-
 136 raphy is unstable.

137 The collision number θ has a second interpretation that is related to mathemat-
 138 ical theories of bedform initiation. Specifically, it is an inverse Knudsen number quan-
 139 tifying whether continuum descriptions of transport are permissible for modeling fluc-

140 tuations in the transport rate at lengthscales that are proportional to the mean parti-
 141 cle hop distance (Furbish, 1997; Furbish et al., 2017; Rapp, 2017). This interpretation
 142 is critical because most formulations of the linear stability problem involve continuum
 143 models that express the transport rate as a function of topography and the turbulence-
 144 averaged flow field. As a result, they implicitly assume that deviations from the statis-
 145 tically expected transport rate can be ignored. In reality, lower-stage plane bed topog-
 146 raphy is stable under conditions where sediment transport is known to be highly inter-
 147 mittent (Furbish et al., 2017; Pähtz et al., 2020), exhibiting large fluctuations that are
 148 potentially consequential to the stability problem (Ancey, 2010; Ancey & Heyman, 2014).
 149 We show that continuum-based morphodynamic models break down at the most unsta-
 150 ble wavelength predicted from linear stability theory at approximately $\theta = 1$ and hy-
 151 pothesize that lower-stage plane bed topography is an outcome of rarefied transport pro-
 152 cesses.

153 We present two proof-of-concept tests that support the hypothesized connection
 154 between particle collisions, bedload rarefaction, and lower-stage plane bed topography.
 155 First, we estimate θ from experimental observations of particle motion over stable and
 156 unstable planar topography by assuming bedload particles behave like molecules in an
 157 ideal gas. Although this assumption is not strictly valid, the basic comparison of scales
 158 may explain why numerous authors over the past century have suggested interactions
 159 between moving particles drive a shift in the balance between disturbance growth and
 160 relaxation (e.g., Bagnold, 1935; Langbein & Leopold, 1968; P. B. Williams & Kemp, 1971;
 161 Costello, 1974; Coleman & Melville, 1994; Coleman & Nikora, 2009). Results of this test
 162 reveal that the transition corresponds to a large increase in θ from $\theta < 1$ to $\theta > 1$.
 163 Second, we incorporate existing empirical formulae to predict θ as a function of hydraulic
 164 and sedimentary boundary conditions. This enables a comparison with databases reported
 165 by previous studies and leads to a predicted threshold of bedform initiation that mir-
 166 rors classic empirical stability diagrams (Southard & Boguchwal, 1990; van den Berg &
 167 van Gelder, 1993; Carling, 1999). Overall, our results suggest that (a) lower-stage plane
 168 bed topography is an outcome of rarefied, intermittent transport and (b) particle col-
 169 lisions play a critical role in the bedform initiation process.

170 2 Theory

171 Here, we derive an expression for θ using a simplified, probabilistic model for bed-
 172 load particle motion under statistically steady, uniform macroscopic transport conditions
 173 (Furbish, Haff, et al., 2012). This expression serves several purposes. First, it reveals an
 174 important connection between particle collisions and transport rarefaction. Second, it
 175 enables estimation of θ using variables that can be extracted from experimental mea-
 176 surements of tracer particle motion discussed in section 3. Finally, the expression for θ
 177 is combined with existing empirical transport formulae to estimate θ as a function of the
 178 macroscopic state variables that govern particle motion (section 4), enabling a direct com-
 179 parison with observations of lower-stage plane bed topography and bedforms that inform
 180 classic empirical stability diagrams (Southard & Boguchwal, 1990; van den Berg & van
 181 Gelder, 1993; Carling, 1999).

182 Our approach is based on the assumption that inter-particle collisions may be pre-
 183 dicted through analogy to kinetic gas theory in two dimensions (Kauzmann, 2012). We
 184 recognize that there are substantial differences between gases and bedload transport. In-
 185 deed, many studies document correlations in particle position and velocity that violate
 186 the assumptions of kinetic theory (e.g., Ancey & Heyman, 2014; Heyman et al., 2014),
 187 and mathematical models for bedload transport have been proposed that invoke analo-
 188 gies to other phenomena (e.g., Aussillous et al., 2013; Houssais et al., 2016; Aussillous
 189 et al., 2016). The analogy to kinetic theory is made here because it represents the sim-
 190 plest possible model that leads to a well-defined estimate of the collision frequency in
 191 a field of particles with randomized positions and velocities. Although there are elements

192 of particle motion that are not captured by this analogy, we suggest that the compar-
 193 ison of scales outlined below provides an approximate description of a transport thresh-
 194 old that has been described in a variety of contexts (e.g., partial/full mobility, intermit-
 195 tent/continuous transport). Ultimately, every mathematical model incorporates simpli-
 196 fications of physical processes and must ultimately be evaluated by its ability to explain
 197 certain phenomena of interest. Below, we show that this analogy quantifies a critical trans-
 198 port threshold that occurs under conditions that are similar to transport thresholds de-
 199 scribed by other authors (e.g., Wilcock & McArdell, 1997; González et al., 2017; Pfeif-
 200 fer & Finnegan, 2018; Pähtz et al., 2020) while providing a conceptual link between de-
 201 scriptive and mathematical theories of bedform initiation. We argue that the overall com-
 202 patibility of this simple model for particle collisions with many disparate observations
 203 and ideas indicates that it is sufficient to describe an important underlying physical phe-
 204 nomenon.

205 Throughout this study (including above), we focus primarily on count-based de-
 206 scriptions of particle motion like the entrainment frequency E_g ($L^{-2}T^{-1}$) opposed to vol-
 207 umetric quantities like the entrainment rate E (LT^{-1}). Count-based (granular) quan-
 208 tities are denoted by the subscript g , and are related to volumetric quantities by the par-
 209 ticle volume $V_p = \pi D^3/6$, where D (L) is the nominal particle diameter. For example,
 210 the volumetric particle activity γ (the average volume of moving particles per unit bed
 211 area) is related to the granular activity γ_g (the average number of moving particles per
 212 unit bed area) as $\gamma = V_p \gamma_g$.

213 In order to estimate the collision frequency for mobile bedload particles, we con-
 214 sider the circular projections of identical spherical particles moving in a two dimensional
 215 plane with randomized positions and velocities. In this scenario, kinetic theory predicts
 216 that the collision frequency for a single particle z_g (L^{-2}) is given by

$$z_g = 2D\gamma_g \langle |\tilde{\mathbf{u}}| \rangle. \quad (1)$$

217 Here, D (L) is the particle diameter and $\langle |\tilde{\mathbf{u}}| \rangle$ (LT^{-1}) is a collision velocity equal to the
 218 average magnitude of the vector difference in velocities between two randomly selected
 219 mobile particles. In an ideal gas, particles have a mean velocity of zero and follow a isotropic
 220 joint normal distribution. Integrating over the joint probability distribution of particle
 221 velocity for two independent particles leads to a collision velocity that is related to the
 222 mean particle speed $\langle |\mathbf{u}| \rangle$ as $\langle |\tilde{\mathbf{u}}| \rangle = \sqrt{2} \langle |\mathbf{u}| \rangle$.

223 One important difference between bedload particle motions and gas molecules is
 224 that bedload particles are advected primarily in one direction. As a result, lateral motions
 225 are small, upstream motions are rare, and downstream velocities are positively skewed.
 226 The effect of this overall behavior on the collision frequency can be estimated by sub-
 227 stituting the isotropic joint normal distribution describing ideal gas molecule velocities
 228 with an appropriate model for the joint distribution of longitudinal and lateral bedload
 229 particle velocities. Neglecting lateral velocities and assuming longitudinal velocities fol-
 230 low an exponential distribution (Fathel et al., 2015; Furbish et al., 2016) leads to

$$\langle |\tilde{\mathbf{u}}| \rangle = \langle u \rangle, \quad (2)$$

231 where $\langle u \rangle$ is the mean longitudinal particle velocity. This simplification is verified be-
 232 low using measurements of tracer particle motion (section 3.6). In this case, collisions
 233 only occur because fast-moving particles overtake slow-moving particles, which is entirely
 234 consistent with descriptions of particle interactions reported by Coleman and Nikora (2009).

235 The collision frequency per unit bed area Z_g is computed from the collision frequency
 236 for a single particle by assuming there are γ_g identical moving particles per unit bed area,
 237 each experiencing collisions with frequency z_g . This leads to

$$Z_g = \gamma_g z_g = 2D\gamma_g^2 \langle u \rangle, \quad (3)$$

238 Note that each collision event is counted twice (once for each particle involved in the col-
 239 lision) so that $\theta = Z_g/E_g$ represents the average number of collisions that a particle
 240 experiences in transit from entrainment to disentrainment.

241 From (3), θ may be estimated from parametric descriptions of particle motion as:

$$\theta = \frac{2D\gamma_g^2\langle u \rangle}{E_g} \quad (4)$$

242 Next, θ is shown to be an inverse Knudsen number (the ratio of the mean free path to
 243 a characteristic lengthscale) by substituting the following statements:

$$E_g = \frac{\gamma_g}{T_p} \quad (5)$$

$$L_x = \langle u \rangle T_p \quad (6)$$

244 where T_p is the mean particle travel time. These statements are valid under statistically
 245 steady, uniform macroscopic flow conditions (Furbish, Haff, et al., 2012). Finally, not-
 246 ing that the mean free path for particles moving in a two dimensional plane is given by
 247 $\lambda = [2D\gamma_g]^{-1}$ (Kauzmann, 2012), θ becomes
 248

$$\theta = 2D\gamma_g\langle u \rangle T_p = L_x/\lambda. \quad (7)$$

249 Henceforth, we refer to conditions where $\theta < 1$ as the “rarefied regime”, and $\theta > 1$ as
 250 the “collisional” regime. A schematic interpretation of this expression is presented in Fig-
 251 ure 2.

252 The Knudsen number quantifies whether continuum approximations are permis-
 253 sible for describing fluctuations in transport rate over a specific lengthscale of interest
 254 (Furbish, 1997; Furbish et al., 2017; Rapp, 2017). Specifically, continuum models are per-
 255 missible at a lengthscale L_c when $\lambda/L_c \ll 1$. Noting that the fastest growing wavelength
 256 predicted from linear stability analysis λ_i is thought to scale with a saturation length
 257 that is related to the particle hop distance L_x as a nearly constant proportion of $\lambda_i/L_x =$
 258 $O(10)$ in the transitional disturbance regime (Andreotti et al., 2002; Charru et al., 2013),
 259 it follows that continuum models for transport are permissible at the scale of the initial
 260 instability λ_i when $\theta \gg 0.1$. Although the failure of continuum models is gradual rather
 261 than abrupt, we argue that $\theta = O(1)$ provides a rough approximation of when this tran-
 262 sition should occur.

263 In summary, the quantity θ has two interpretations. First, it is an estimate of the
 264 average number of collisions per particle hop, quantifying as transition in collective par-
 265 ticle behavior that is qualitatively aligned with transport thresholds described in other
 266 contexts (Wilcock & McArdell, 1997; Pähtz et al., 2020). This interpretation is aligned
 267 with descriptive studies that suggest particle collisions drive a shift in the balance be-
 268 tween granular disturbance growth and relaxation (Bagnold, 1935; Langbein & Leopold,
 269 1968; Costello, 1974; Coleman & Melville, 1994; Coleman & Nikora, 2009, 2011). Sec-
 270 ond, it is an inverse Knudsen number quantifying the degree of rarefaction at the scale
 271 of individual particle motions. This interpretation may explain why most theoretical sta-
 272 bility analyses fail to predict that planar topography is stable under weak bedload trans-
 273 port conditions: planar topography is an outcome of rarefied transport processes that
 274 occur below the resolution of continuum models that depend on the statistically expected
 275 transport rate.

276 With these interpretations in mind, we reiterate that (4) and (7) depend on assump-
 277 tions that are not strictly valid for bedload transport. Collective entrainment effects (Ancey,
 278 2010; Heyman et al., 2014) cause correlations in particle activity that reduce the effec-
 279 tive distance most particles can travel before colliding with another particle relative to
 280 λ . At the same time, spatiotemporal correlations in the velocities of moving particles driven

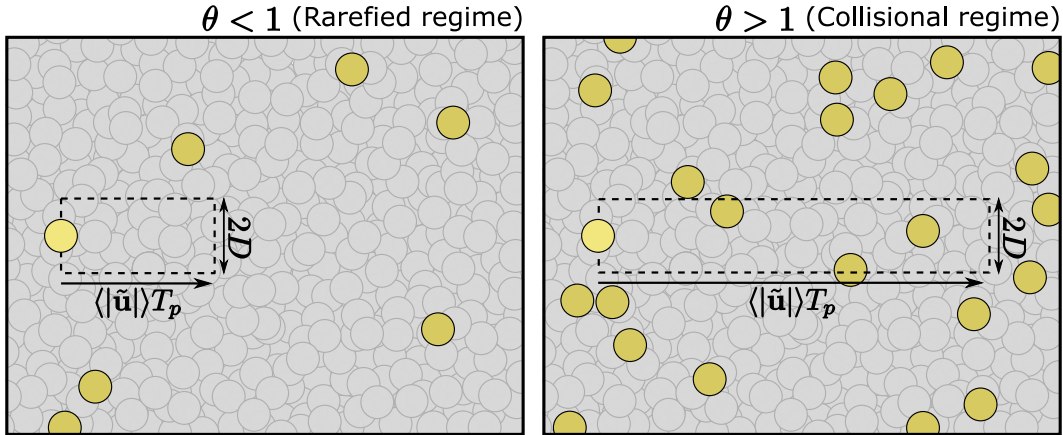


Figure 2. Schematic illustrating rarefied ($\theta < 1$) and collisional ($\theta > 1$) transport conditions. Mobile particles are shown in yellow, and immobile particles are shown in grey. A typical particle (light yellow) sweeps out a rectangle with area $2D \times \langle |\tilde{\mathbf{u}} | \rangle T_p$ during its transit from entrainment to disentrainment. The collision number θ may be interpreted as the average number of particles contained within this rectangle as a function of γ_g .

281 by a fluid will cause a decrease in the velocity difference between colliding particles relative to $\langle |\tilde{\mathbf{u}} | \rangle$. While both of these effects influence the true collision frequency for bedload particles, we suggest that these are second-order effects at low transport stages and that kinetic theory provides a reasonable first-order estimate that is sufficient to constrain a possible connection between bedload rarefaction, particle collisions, and bed configuration. The remainder of this paper is focused on evaluating whether theory presented here can explain observations of particle motion and bed configuration under weak bedload transport conditions.

289 3 Experimental Observations of Particle Motion

290 3.1 Description of Experiments

291 In this section, we investigate grain-scale transport processes under two experimental conditions characterized by (a) stable and (b) unstable planar topography. The goal of this exercise is to evaluate whether measurements of particle motion lead to estimates of θ that are compatible with our hypothesis.

292 Experiments were conducted in a 1.19 m wide, 14 m long flume capable of recirculating sediment and water. Flow conditions in the flume could be adjusted by varying (a) the water discharge, (b) the flow depth at the downstream end. The flume slope can also be adjusted, but the bed surface slope may vary with respect to the flume slope and is expected to adjust to an equilibrium value set by the discharge and outlet depth (Parker & Wilcock, 1993). Recognizing this, we chose to vary flow conditions by changing the water discharge while holding the outlet flow depth (12 cm) and flume slope (0.001) constant. This allowed for variation in the bed stress while maintaining a roughly constant relative submergence (the ratio of flow depth to grain size).

293 The bed material was composed of polystyrene particles with a geometric mean diameter of 2.1 mm and a density of 1.055 g/cm³. The base-2 logarithmic standard deviation of the grain size distribution was 0.32 (68% of the bed material had a diameter within a factor of $2^{0.32} = 1.24$ of the geometric mean), which is narrower than most naturally-sorted sediments. The dimensionless particle Reynolds number ($Re_p = \sqrt{gRD^3}/\nu$, where

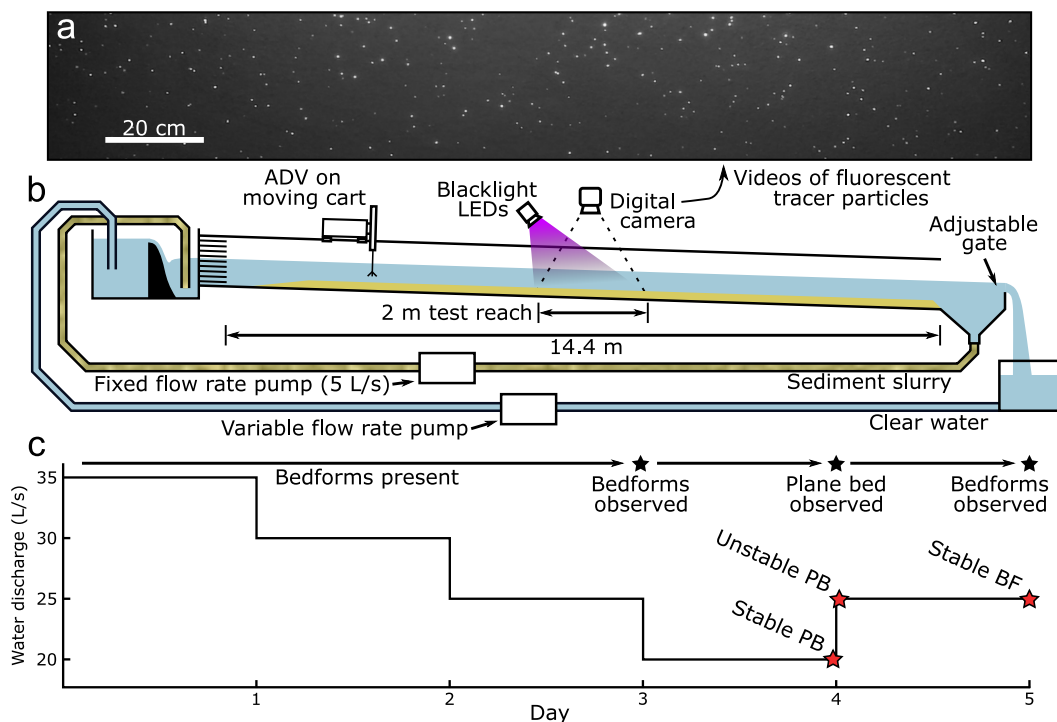


Figure 3. Schematic showing an image of fluorescent tracer particles (a), the experimental setup (b) and a timeline of the experiment (c). Red stars in the timeline indicate data collection events. Reported particle tracking data were collected over stable and unstable planar topography (labeled "Stable PB" and "Unstable PB"). Reported measurements of bedform geometry were collected over stable bedforms ("Stable BF").

309 R is the submerged specific gravity of the sediment, ν is the kinematic viscosity of the
 310 fluid, and g is gravitational acceleration) was approximately 70.7, which is equivalent to
 311 quartz sand ($R = 1.65$) with diameter $D = 0.68$ mm. This material covered the bed
 312 of the flume in a layer that was approximately 15 cm thick.

313 In order to achieve flow conditions straddling the threshold of bedform develop-
 314 ment, we initially allowed topography to equilibrate to a discharge known to produce bed-
 315 load dominated bedforms (35 L/s). Then, we incrementally reduced the discharge by 5
 316 L/s, allowing the bed to adjust for 24 hours after each reduction in discharge, until pla-
 317 nar topography was observed. This occurred at 20 L/s. Because the planar topography
 318 was formed by the flow from an initially dune-covered bed, we are confident that it was
 319 a stable equilibrium configuration. Measurements of bed topography and particle moti-
 320 on were collected over equilibrium lower-stage plane topography as described in more
 321 detail below. Discharge was then increased to 25 L/s and identical measurements were
 322 immediately made over unstable plane bed topography. Finally, the bed configuration
 323 was allowed to equilibrate to the increased water discharge for roughly 24 hours to ver-
 324 ify the presumed instability and topography was measured a third time.

325 Bed elevation profiles were measured using Nortek Vectrino Profiler acoustic Doppler
 326 velocimeter (ADV). The ADV was mounted to a moving cart and moved upstream and
 327 then back downstream along a 2 m longitudinal transect in the center of the flume at
 328 a speed of 3.8 cm/s. 6 scans of bed topography were collected for each experimental con-
 329 dition. Bed elevation profiles indicate that the total variation in bed elevation was ap-
 330 proximately $3D$ were under stable and unstable plane bed conditions. We neglect these

331 small bed defects in terms of their effect on macroscopic particle motion statistics. Al-
 332 though particle motion may exhibit conditional dependence on position with respect to
 333 bed defects, we assume that measured quantities reflect marginal distributions of par-
 334 ticle motion (i.e. averaged over all possible positions relative to bed defects) that are rel-
 335 evant to the long-term evolution of bed configuration.

336 After the bed was allowed to equilibrate to the 25 L/s water discharge condition
 337 for 24 hours, we observed well-developed “3D” dunes (*sensu* Venditti et al., 2005b) with
 338 measured lee slopes at the angle of repose (maximum 35 degrees). Two bedform crests
 339 were visually identified in six repeat longitudinal profiles collected at 105 second inter-
 340 vals. These profiles covered 2 m of the bed at a spatial resolution of 1 cm. Bedform length
 341 computed as the average distance between the highest point of the crests in all six scans
 342 was 64 cm. The bedform height computed as the average height from the highest point
 343 of each crest to the lowest point before the next crest was 2.9 cm. The migration veloc-
 344 ity estimated by averaging the displacement of the individual crests between scans was
 345 1.4 cm/minute. Although more sophisticated methods exist for quantifying the charac-
 346 teristic scales of bedform topography, these basic geometric quantities are sufficient for
 347 our purposes.

348 3.2 Flow Conditions

349 The primary measure of flow strength reported here is the dimensionless bedload
 350 number $q_* = q_b/\sqrt{gRD^3}$. This is appropriate because our hypothesis leads to a pre-
 351 dicted threshold of bedform development that may be expressed in terms of q_* (section
 352 4). As a result, the threshold stress associated with the critical value of q_* is then es-
 353 timated using empirical formulae (Brownlie, 1981; Wong & Parker, 2006; Recking, 2013).
 354 By estimating τ_* using the same approach, we quantify the relative magnitude of the ex-
 355 perimental stress and the critical stress in a manner that is not sensitive to uncertain-
 356 ties associated with these empirical formulae. This exercise enables a comparison with
 357 observations reported by other authors (Figure 8), however we emphasize that precise
 358 estimates of τ_* are not critical to the hypothesis test presented in this section.

359 In order to provide a basic estimate of τ_* to compare our experimental conditions
 360 with other studies, we first estimate the $\tau_* - \tau_{*c}$ from q_* using the Wong & Parker (2006)
 361 bedload transport formula. Then, we estimate τ_* using a value of $\tau_{*c} = 0.032$ computed
 362 from the empirical curve of Brownlie (1984). Each of these measures of flow strength are
 363 reported in Table 1.

364 As mentioned previously, the equilibrium bed surface slope depends on the water
 365 discharge and outlet flow depth. In order to achieve this state, the flume must be run
 366 under fixed boundary conditions for a sufficient duration to regrade the bed to the equi-
 367 librium slope (Parker & Wilcock, 1993). Due to the relatively short durations and low
 368 transport rates in our experiments, we expect that backwater hydrodynamics influence
 369 the flow strength in the control area. This has two important implications. First, the
 370 friction slope (which scales the bed stress) is expected to deviate from the bed surface
 371 slope, water surface slope, and flume slope. Though the friction slope could be estimated
 372 from the backwater equation if the bed surface and water surface slopes are known, ac-
 373 curate measurement of these quantities is challenging. As a result, double-averaged (time
 374 and space) measurements of sediment load provide a more reliable proxy for flow strength
 375 than a depth slope product using any of these quantities. Second, the flow strength is
 376 expected to vary across the control area. We argue that the longitudinal changes in stress
 377 can be ignored in our experiments because the backwater length $L_{bw} = HS_b$ is much
 378 larger than the length of the control area for reasonable values of S_b , the bed surface slope.
 379 To illustrate this point, we perform a simple calculation to estimate the change in stress
 380 across the control area by extrapolating the stress gradient predicted from the backwa-
 381 ter equation $dH/dx = (S_b - S_f)/(1 - Fr^2)$ (Chaudhry, 1993). Noting that $\tau_* = q_w/(gRC_z H)$,

382 the backwater equation leads to

$$\frac{d\tau_*}{dx} = -\frac{\tau}{H} \frac{S_b - S_f}{1 - Fr^2}. \quad (8)$$

383 The change in stress $\Delta\tau_*$ across the control area length L_{tr} can be estimated by extrap-
 384 olating the local gradient as $\Delta\tau_* = L_{tr}(d\tau_*/dx)$, and the fractional change in stress $|\Delta\tau_*|/\tau_*$
 385 is given by

$$\frac{|\Delta\tau_*|}{\tau_*} = \frac{L_{tr}}{H} \frac{|S_b - S_f|}{1 - Fr^2}. \quad (9)$$

386 The friction slope can be estimated for both experimental conditions using the stresses
 387 estimated above and the depth measured in the control area using a ruler through the
 388 side of the flume (approximately 11 cm for both conditions) as $S_f = \tau_*RD/H$. This
 389 leads to $S_f = 5.1 \times 10^{-5}$ for the stable plane bed condition and $S_f = 8.94 \times 10^{-5}$ for
 390 the unstable plane bed condition. Though the bed surface slope is not known, we ex-
 391 pect that it lies somewhere between the flume slope and zero. Under this assumption,
 392 the bed stress can vary by a maximum of 1.8% of its magnitude across the control area
 393 in either experiment. If it is further assumed that the bed slope was in equilibrium with
 394 the flow conditions prior to the increase in water discharge from 20 L/s to 25 L/s, ($S_b =$
 395 S_f), the estimated change in stress across the 2m long control area is 0.07 % of its mag-
 396 nitude for the unstable plane bed condition. Although many elements of this calcula-
 397 tion are poorly constrained (for example, the measured flow depth in the control area),
 398 it serves to demonstrate that the basic assumption of longitudinally uniform flow is ap-
 399 proximately valid despite the fact that backwater hydrodynamics influence the stress.
 400 We note also that observations of particle motion support this assumption: particle be-
 401 havior exhibited marked qualitative differences between the two experimental conditions
 402 but did not vary noticeably in the longitudinal direction, even outside of the control area
 403 (Figure 4).

404 3.3 Particle Tracking

405 Parameters describing the kinematic properties of particle motion were extracted
 406 from manually-digitized tracer particle paths. To this end, a small fraction of the bed
 407 material was removed from the flume and coated with a thin layer of fluorescent spray
 408 paint. These particles were then added back to the flume and allowed to mix with the
 409 bed material under a range of flow conditions prior to these experiments. Illuminating
 410 the bed with a blacklight increases the contrast of tracer particles relative to other par-
 411 ticles so that individual particles can be confidently tracked over long durations. This
 412 procedure also significantly reduces the number of particles that need to be tracked in
 413 order to obtain a representative sample of particle behavior (Naqshband et al., 2017; Ash-
 414 ley, Mahon, et al., 2020).

415 Videos of tracer particle motion were recorded using a downward facing digital cam-
 416 era attached to a fixed boom 2.05 m above the water surface. Because the flow veloc-
 417 ities needed to mobilize the polystyrene particles were low relative to quartz sand, par-
 418 ticles could be tracked through the water surface with a high degree of precision. Im-
 419 age rectification (which corrects for image distortion due to slight misalignment of the
 420 camera), and registration (which establishes a coordinate system in the correct units al-
 421 lowing for conversion from pixel position to bed position) were performed with known
 422 reference points in the flume using OpenCV (Bradski, 2000) in Python. Manual digiti-
 423 zation of particle motions was performed using TrackMate (Tinevez et al., 2017), an open
 424 source particle tracking package for ImageJ (Schindelin et al., 2012). In order to min-
 425 imize sampling bias, all tracer particle motions that occurred within the sampling win-
 426 dow during the specified time interval were tracked. Two ten second videos comprising
 427 a total of twenty seconds of observations from each experiment were used for this study.
 428 After registration, rectification, and trimming, both videos covered a streamwise distance
 429 of 210 cm and a cross-stream distance of 99 cm. Particle behavior is sensitive to inevitable

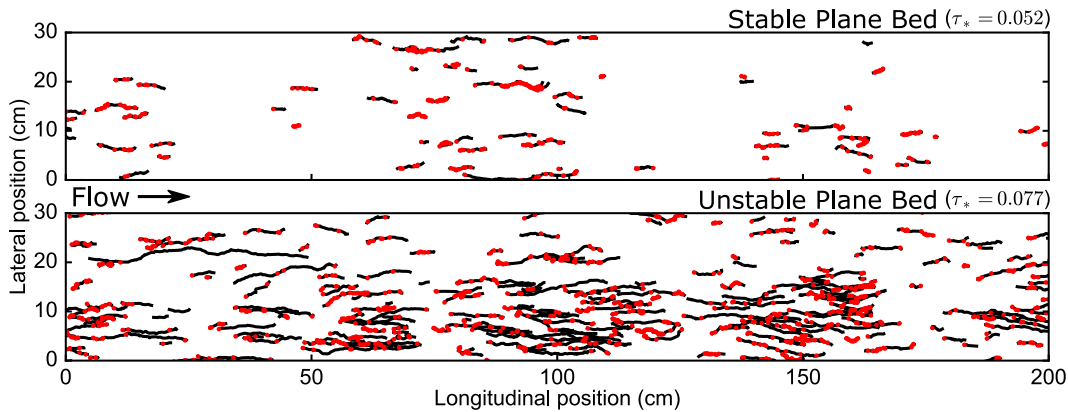


Figure 4. Tracer particle paths (black lines) and entrainment event locations (red dots) for stable and unstable plane bed conditions. Data are from the same total duration for both experiments (20 s) such that apparent differences in the densities of black lines and red dots are representative of the relative sediment loads and entrainment frequencies.

430 variations in shear stress that occur in the cross-stream direction (Abramian et al., 2019).
 431 For this reason, analyses reported here were performed using particle motions that oc-
 432 curred within a 30 cm wide, 2 m long control volume in the center of the flume corre-
 433 sponding to the location where shear stress was estimated from flow velocity measure-
 434 ments. We note that the initial phase of bedform growth began in this region and then
 435 propagated laterally to the edges of the flume. Tracked particle paths are plotted in Fig-
 436 ure 4. Reported parametric descriptions of particle motion were computed from digitized
 437 tracer particle paths using the procedure described in 3.4.

438 Videos were recorded at a framerate of 30 Hz and a resolution of roughly 9.4 pix-
 439 els per cm at the bed surface. Videos were downsampled to a resolution of 4.7 pixels per
 440 cm so that raster data could be stored without compression in computer memory. Af-
 441 ter rectification and registration, the length of each pixel was 2.1 mm (approximately
 442 the nominal particle diameter). Fluorescent tracer particles create a halo that illuminates
 443 adjacent pixels, and differences in pixel brightness enable robust estimation of the par-
 444 ticle centroid location at sub-pixel resolution (Leary & Schmeeckle, 2017).

445 Particle tracking software records particle location with an arbitrary degree of pre-
 446 cision depending on image magnification; thus, particles which are qualitatively identi-
 447 fied as immobile may possess nonzero measured velocities. Following previous studies
 448 (e.g., Lajeunesse et al., 2010; Liu et al., 2019; Ashley, Mahon, et al., 2020), we employed
 449 a velocity threshold criteria to distinguish mobile and immobile particles. Velocity cri-
 450 teria are useful because they provide a reproducible solution to this problem, and be-
 451 cause sensitivity analysis can easily be conducted by varying the value of the velocity
 452 threshold. For additional discussion of velocity criteria, see Ashley, Mahon, et al. (2020)
 453 and references therein. Recognizing that the motion state of certain particles is unclear,
 454 we inspected motions identified using a range of velocity thresholds and found that vi-
 455 sual identification of particle motion corresponded to values of the velocity threshold rang-
 456 ing from $u_c = 0.005$ m/s to $u_c = 0.01$ m/s. Below 0.005 m/s, particles which remain
 457 in the same location for significant durations are identified as immobile, and above 0.01 m/s,
 458 particles which are clearly in motion in the bedload phase are identified as immobile. The
 459 exact values of certain computed quantities are sensitive to the specific choice of veloc-
 460 ity threshold within this range; however, the primary findings of this work are not. Re-
 461 ported results were obtained using a velocity threshold of 0.007 m/s, which is approx-
 462 imately the geometric midpoint of the optimum range (0.005 m/s to 0.01 m/s).

In order to compute certain bulk statistics of sediment transport from tracer particle statistics, it was necessary to estimate the tracer fraction in the flume. This was accomplished by collecting a sample of material within a few centimeters of the bed surface from three locations spread across the bed after the experimental campaign was complete. Tracer particles are expected to be evenly distributed in this region due to the migration of bedforms. The total mass of the sample was 760 g. Tracer particles were separated by hand under a blacklight and then weighed. The total mass of tracer particles in the sample was 1.49 g. Thus, we estimate the tracer fraction to be 0.00196.

3.4 Methods for Computing Particle Motion Statistics From Digitized Particle Paths

3.4.1 Particle Position and Velocity

The kinematic statistics of particle motion needed to estimate θ using equation (4) were computed from digitized particle paths following Ballio et al. (2018). We consider digitized particle motions within a control volume extending from the flume bottom to the water surface projected onto a 2 dimensional plane A (Figure 4). Each particle motion is defined by a sequence of discrete measurements of particle position on the domain of longitudinal position x and lateral position y . The position of the i^{th} of m tracked particles in the t^{th} of n frames is expressed by the vector $\mathbf{x}_{i,t}$ with longitudinal and lateral components $x_{i,t}$ and $y_{i,t}$.

Particle velocities are computed by comparing subsequent positions of a particle. Measured velocities therefore represent temporal averages between the two measurements of particle position; however, the time between frames δt is sufficiently small that it may be viewed as an instantaneous velocity for our purposes. This assumption may be evaluated by comparing δt to the timescales characterizing fluctuations in particle velocity. Furbish, Ball, and Schmeeckle (2012) argue that the velocity signal must possess a fundamental harmonic with period $T = 2T_p$, implying that in the most basic sense, the mean particle travel time sets the primary scale of fluctuations in particle velocity. We estimate $T_p \gg \delta t$ for both experiments.

The velocity vector $\mathbf{u}_{i,t}$ with longitudinal and lateral components $u_{i,t}$ and $v_{i,t}$ is computed as

$$\mathbf{u}_{i,t} = \frac{\mathbf{x}_{i,t+1} - \mathbf{x}_{i,t}}{\delta t}. \quad (10)$$

Thus, the velocity attributed to frame t represents the average velocity between frame t and frame $t + 1$.

3.4.2 Mean Granular Activity γ_g

The mean granular activity is computed by counting the number of active tracer particles in the control volume in each frame and averaging. This is accomplished using an Eulerian clipping function M^A to quantify whether the i^{th} tracer particle is within the control area A in the t^{th} frame:

$$M_{i,t}^A = \begin{cases} 1, & \text{if } \mathbf{x}_{i,t} \in A \\ 0, & \text{otherwise} \end{cases}. \quad (11)$$

Additionally, a velocity threshold u_c is used to define the state of motion of a particle quantified by the clipping function M^m :

$$M_{i,t}^m = \begin{cases} 1, & \text{if } |\mathbf{u}_{i,t}| \geq u_c \\ 0, & \text{otherwise} \end{cases}. \quad (12)$$

Thus, the number of mobile tracer particles in the control volume in frame t is given by:

$$N_t^m = \sum_{i=1}^m M_{i,t}^m M_{i,t}^A. \quad (13)$$

503 Tracer particle positions recorded in n frames lead to $n - 1$ measurements of velocity.
 504 Thus, the average number of moving tracer particles within the control volume over all
 505 frames with valid velocity measurements can be estimated as:

$$\langle N^m \rangle = \frac{1}{n-1} \sum_{t=1}^{n-1} N_t^m. \quad (14)$$

506 Here, angle brackets denote sample averages which provide unbiased estimates of the en-
 507 semble assuming ergodicity.

508 The granular activity is estimated by dividing $\langle N^m \rangle$ by the tracer particle fraction
 509 ψ and the control volume area:

$$\gamma_g = \frac{\langle N^m \rangle}{\psi A}. \quad (15)$$

510 Note that γ_g is an estimate of a mean, but angle brackets are dropped to simplify no-
 511 tation in section 2.

512 **3.4.3 Granular Entrainment Frequency E_g**

513 The final relevant quantity that must be estimated to compute θ with equation (7)
 514 is the entrainment frequency E_g . Entrainment and detrainment events are defined as
 515 transitions between the mobile and immobile states and are quantified by differenti-
 516 ating M^m with respect to time (Ballio et al., 2018). Following this approach, we define an
 517 entrainment/detrainment function $M^{E,D}$ as

$$M_{i,t}^{E,D} = M_{i,t}^m - M_{i,t-1}^m. \quad (16)$$

518 This function may take on values of 1, 0, or -1 , signifying an entrainment event, no event,
 519 or a detrainment event. In order to consider only entrainment events, values of -1
 520 are replaced with 0, producing an entrainment function M^E . The total number of en-
 521 trainment events that occur in the control area during the t^{th} frame is given by

$$N_t^E = \sum_{i=1}^m M_{i,t}^E M_{i,t}^A \quad (17)$$

522 and an estimate of the average number of entrainment events in a frame is given by

$$\langle N^E \rangle = \frac{1}{(n-2)} \sum_{t=2}^{n-1} N_t^E. \quad (18)$$

523 Here, $(n-2)$ is the total number of frames during which it is possible to detect entrain-
 524 ment events occurring in n frames. Finally, the granular entrainment frequency may be
 525 estimated by dividing the average number of entrainment events per frame by the frame
 526 duration:

$$E_g = \frac{\langle N^E \rangle}{\psi A \delta t} \quad (19)$$

527 The mean travel time T_p is estimated from E_g and γ_g using (5). This estimate of T_p is
 528 not biased by particles entering or leaving the control area.

529 **3.5 Uncertainty in Estimates of q_* and θ**

530 Uncertainty in experimental results primarily reflects uncertainty in four param-
 531 eters that are estimated from data. These are (a) the tracer particle fraction ψ , (b) the
 532 average number of moving particles in the control area at any instant $\langle N^m \rangle$ (equation
 533 14), (c) the average number of entrainment events occurring in the control area between
 534 each frame $\langle N^E \rangle$ (equation 18), and (d) the mean particle velocity $\langle u \rangle$. In order to quan-
 535 tify uncertainty in these parameters and propagate results through calculations of θ and

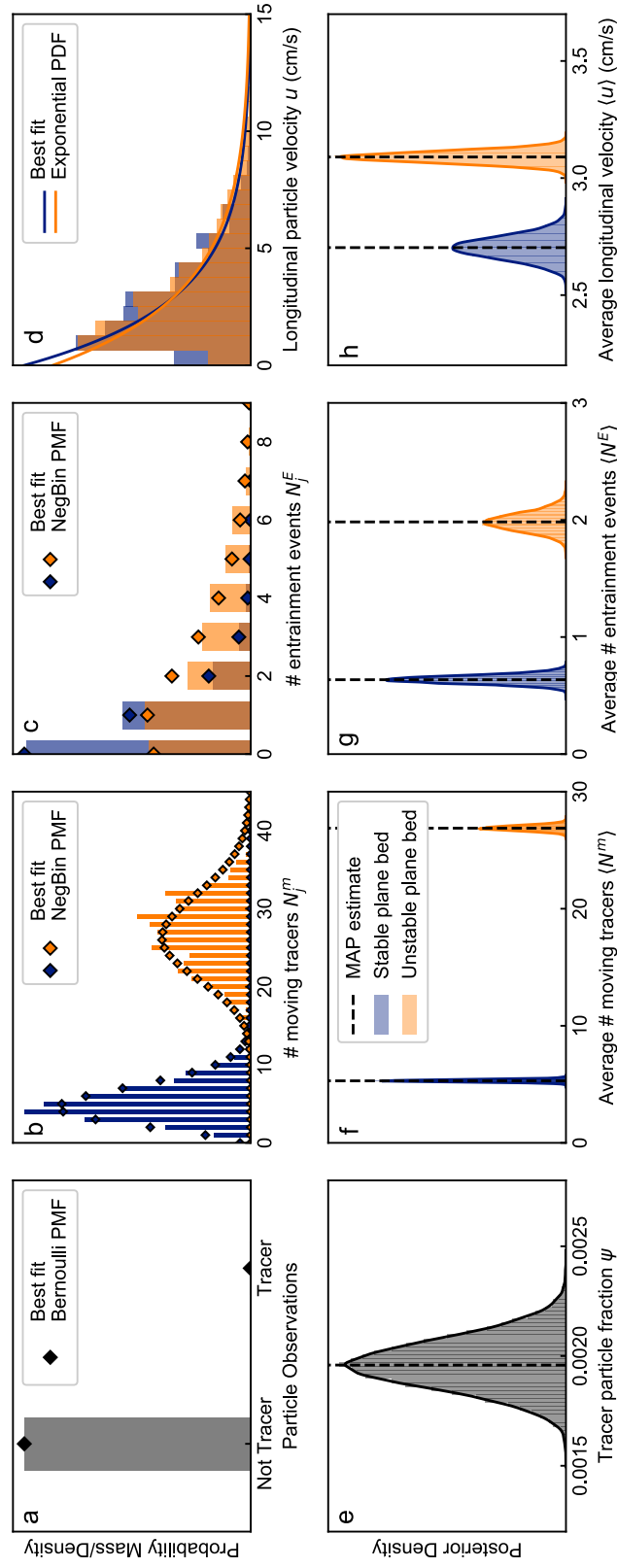


Figure 5. visualization of Bayesian uncertainty analysis. Top panels compare best-fit (Maximum a-posteriori) distributions with data. Bottom panels show maximum a-posteriori estimates and full Bayesian posterior distributions for parameters used to compute θ and q_* .

536 q_* , we fit theoretical distribution models to our data using Bayesian statistical techniques
 537 under the following assumptions:

- 538 • In order to estimate ψ , we assume each sampled particle may be viewed as an in-
 539 dependent Bernoulli trial. The sample size controls the uncertainty and was es-
 540 timated by dividing the sample mass by the particle mass $V_p\rho_s$, where ρ_s is the
 541 sediment density (Figure 5a).
- 542 • We assume the instantaneous number of moving particles in the control area N_t^m
 543 follows a negative binomial distribution (Ancey et al., 2008; Ancey, 2010) with pa-
 544 rameters p and q . These parameters are related to the mean by $\langle N^m \rangle = pq/(1-$
 545 $p)$ (Figure 5b).
- 546 • We assume that the number of entrainment events that occur over a finite time
 547 interval between frames N_t^E follows a negative binomial distribution. Like the av-
 548 erage number of moving particles, the number of entrainment events are expected
 549 to follow a Poisson distribution (a special case of the negative binomial distribu-
 550 tion) if entrainment events are independent. However, we find that the Poisson
 551 distribution provides a poor fit to observations for the unstable plane bed condi-
 552 tion, likely due to collective entrainment effects. While our use of the negative bi-
 553 nomial distribution in this context currently lacks theoretical justification, it rep-
 554 represents a simple way to relax the constraint that the mean is equal to the variance
 555 imposed by the Poisson distribution, leading to an improved fit. Ultimately, the
 556 estimate of the mean and the associated uncertainty is not sensitive to this choice
 557 (Figure 5c).
- 558 • We assume longitudinal particle velocities follow an exponential distribution (Furbish
 559 & Schmeeckle, 2013; Fathel et al., 2015; Furbish et al., 2016) (Figure 5d).

560 Probability distribution models were fit using Markov Chain Monte-Carlo (MCMC) sam-
 561 pling (Christensen et al., 2011) with flat priors. This approach provides a sample drawn
 562 from the posterior distribution that may be used to estimate Bayesian credible intervals
 563 and simulate predictive distributions of other quantities. Probability distributions as-
 564 sociated with maximum a-posteriori estimates of model parameters (which are equiv-
 565 alent in this case to maximum likelihood estimates due to the use of flat priors) are plot-
 566 ted along with their full posterior distributions in Figure 5. Predictive distributions of
 567 q_* and θ (Figure 6) were simulated from MCMC samples of ψ , $\langle N^E \rangle$, $\langle N^m \rangle$, and $\langle u \rangle$ us-
 568 ing the following expressions:

$$q_* = \frac{1}{A\sqrt{gRD^3}} \frac{\langle N^m \rangle \langle u \rangle}{\psi} \quad (20)$$

$$\theta = \frac{2D\delta t}{A} \frac{\langle N^m \rangle^2 \langle u \rangle}{\psi \langle N^E \rangle}. \quad (21)$$

570 These expressions reflect substitution of (15) and (19) into (4) and the activity form of
 571 the flux (Furbish, Haff, et al., 2012). Note that we do not account for uncertainty in the
 572 control area A , gravitational acceleration g , the submerged specific gravity of sediment
 573 R , the particle diameter D or the frame interval δt .

574 3.6 Experimental Results

575 Estimates of mean quantities describing tracer particle motion were computed from
 576 experimental data above using the procedure described in section 3.4. A summary of ex-
 577 perimental conditions and results is reported in Table 3.6. Reported values of q_* and θ
 578 reflect maximum a-posteriori estimates described in section 3.5.

579 For the stable plane bed condition, the experimental procedure described above yielded
 580 a total of 3168 measurements of particle speed in excess of the threshold speed in the
 581 control volume belonging to 70 unique particles (Figure 4). The entrainment function

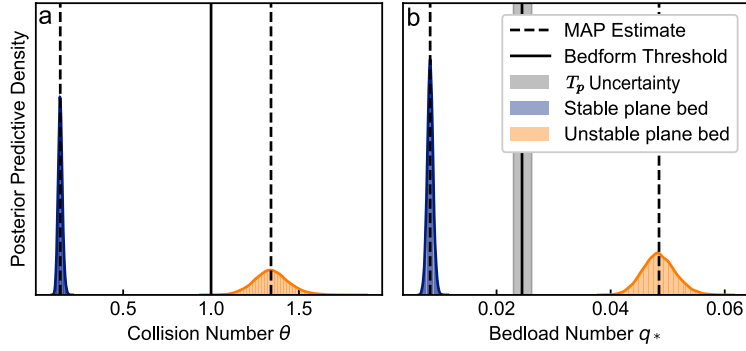


Figure 6. Results of uncertainty analysis described in section 3.5. Maximum a-posteriori estimates and posterior predictive distributions for the bedload number q_* and the collision number θ computed using Bayesian MCMC sampling. Bedform thresholds are given by $\theta = 1$ and equation (25) with $C_d = 4/3$. Grey envelope labeled “ T_p Uncertainty” represents uncertainty related to the prefactor in the travel time equation reported by Lajeunesse et al. (2010) This figure represents the most appropriate estimate of uncertainty in experimental conditions relative to the hypothesized threshold of bedform initiation because none of the plotted quantities depend on an empirical model for bedload flux.

582 (equation 16) was used to identify a total of 798 tracer particle exchanges with the bed
 583 (entrainment and disentrainment events). The ensemble average tracer particle flux was
 584 0.22 particles per second per meter width. This leads to a total granular flux $q_{sg} = 114$
 585 particles per second per meter width and a bedload number $q_* = q_g V_p / \sqrt{RgD^3}$ of 0.0078.
 586 Solving the Wong and Parker (2006) bedload equation for shear velocity using the crit-
 587 ical Shields stress predicted from Brownlie (1981) leads to $u_* = 0.74$ cm/s

588 For the unstable plane bed condition, experiments produced 16075 measurements
 589 of mobile particles in the control volume belonging to 238 unique particles (Figure 4).
 590 The entrainment function identified 2461 exchanges with the bed. The ensemble aver-
 591 age tracer particle flux was 1.4 particles per second per meter width leading to a total
 592 granular flux of $q_{sg} = 688$ particles per second per meter width and a bedload number
 593 of $q_* = 0.047$. The estimated shear velocity is $u_* = 0.98$ cm/s.

594 Measurements of tracer particle motion also allow for verification of the simplifi-
 595 cation of the velocity distribution that leads to equation (2). We find that $\langle |\tilde{\mathbf{u}}| \rangle = 1.1 \langle u \rangle$
 596 for both experimental conditions. As a result, we argue that it is reasonable to neglect
 597 lateral and upstream motions and assume $\langle |\tilde{\mathbf{u}}| \rangle \approx \langle u \rangle$.

598 4 Comparison with Observations of Bed Configuration

599 In section 3, we estimated θ from observations of tracer particle motion to quan-
 600 tify collision behavior for two experimental conditions straddling the threshold of bed-
 601 form development. Here, we incorporate empirical transport formulae to estimate the
 602 value of θ for observations of bed configuration that inform classic stability diagrams (Southard
 603 & Boguchwal, 1990; van den Berg & van Gelder, 1993; Carling, 1999), providing a sec-
 604 ond test of our hypothesis. As a starting point, we substitute the activity form of the
 605 average flux (Furbish, Haff, et al., 2012) in the bedload phase q_b into equation 7. The
 606 activity form of the flux is given by

$$q_b = \gamma \langle u \rangle. \quad (22)$$

Table 1. Summary of Experiments

	Stable plane bed	Unstable plane bed
Boundary Conditions		
Geometric mean particle diameter D	2.1 mm	2.1 mm
Sediment density ρ_s	1.055 g/cm ³	1.055 g/cm ³
Particle Reynolds Number Re_p	70.7	70.7
Unit water discharge q_w	0.016 m ² /s	0.021 m ² /s
Flow depth in control area h	0.11 m	0.11 m
Estimated Shields stress τ_*	0.049	0.084
Estimated shear velocity u_*	0.0074 m/s	0.0098 m/s
Results		
Granular activity γ_g	4500 m ⁻²	23,800 m ⁻²
Mean relative speed $\langle \tilde{\mathbf{u}} \rangle$	2.9 cm/s	3.3 cm/s
Mean longitudinal velocity $\langle u \rangle$	2.7 cm/s	3.1 cm/s
Entrainment frequency E_g	16000 m ⁻² s ⁻¹	50000 m ⁻² s ⁻¹
Mean travel time T_p	0.26 s	0.43 s
Granular sediment flux q_{sg}	121 m ⁻¹ s ⁻¹	703 m ⁻¹ s ⁻¹
Volumetric sediment flux q_s	5.88×10^{-7} m ² /s	3.41×10^{-6} m ² /s
Collision frequency Z_g	2300 m ⁻² s ⁻¹	67000 m ⁻² s ⁻¹
Bedload number q_*	0.0083	0.048
Mean free path λ	5.3 cm	1.0 cm
Characteristic transport length L_c	0.8 cm	1.4 cm
Collision number θ	0.14	1.33

607 Recall that the volumetric and granular activity are related by the particle volume as
 608 $\gamma = \gamma_g V_p$. This leads to

$$\theta = \frac{12q_b T_p}{\pi D^2}. \quad (23)$$

609 Next, we consider an empirical relation for the mean particle travel time T_p . Lajeunesse
 610 et al. (2010) reviewed previous work and concluded based on physical and dimensional
 611 arguments that the mean travel time should be predicted as

$$T_p = \beta \frac{D}{\omega_s} \left(\frac{u_* - u_{*c}}{\omega_s} \right)^\varepsilon \quad (24)$$

612 where ω_s is the particle settling velocity, u_* is the shear velocity, u_{*c} is the critical shear
 613 velocity for sediment motion, and β and ε are empirical coefficients. Based on available
 614 data, they suggest that $\beta = 10.7 \pm 0.7$ and $\varepsilon = 0$, removing the dependence on u_* .
 615 We recognize that the particle travel time may possess a weak dependence on u_* despite
 616 this result. However, this does not affect the present analysis as a nonzero value of ε does
 617 not influence the trends in θ as a function of τ_* and Re_p (we return to this point below).
 618 The settling velocity is given by $\omega_s = \sqrt{4RgD/3C_d}$, where C_d is a drag coefficient. Com-
 619 bining equations (23) and (24) with the suggested value for β and ε leads to

$$\theta = (35.4 \pm 2.3) \sqrt{C_d q_*}. \quad (25)$$

620 Next, we incorporate the bedload transport formula of Recking (2013), given by

$$q_* = \frac{14\tau_*^{2.5}}{1 + (\tau_{*c}/\tau_*)^4}. \quad (26)$$

621 These authors propose a form for τ_{*c} that incorporates slope and sorting, however this
 622 information is not universally available for the data reported by (Carling, 1999). Instead,

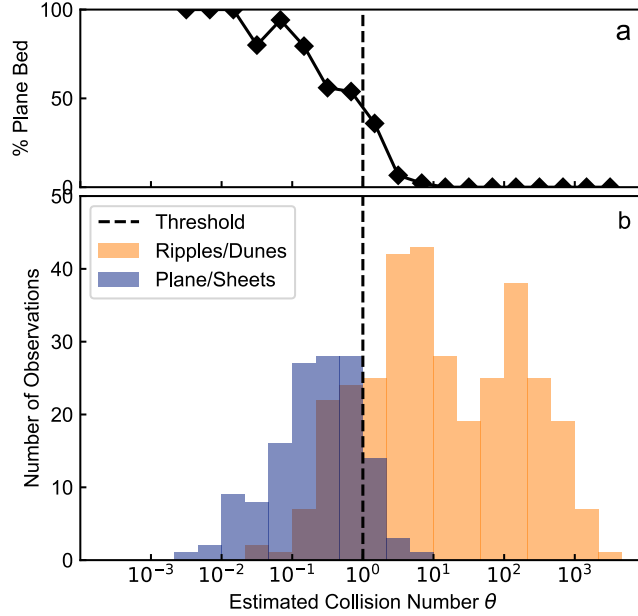


Figure 7. Plot comparing the number of observations of planar topography and bedforms at different estimated values of the collision number θ (equation 27). Panel (a) shows the percentage of observations with in a given range of θ where planar topography was observed. Panel (b) shows the total number of observations of each bed configuration. Although there is substantial overlap in observations of planar topography and bedforms, the most commonly observed bed configuration shifts from planar topography to bedforms at $\theta \approx 1$.

623 we consider $\tau_{*c} = f(Re_p)$ after Brownlie (1981). This approach leads to a predicted value
 624 of τ_* corresponding to $\theta = 1$ that is almost identical to the simpler formula of Wong
 625 and Parker (2006) but more appropriately characterizes small transport rates at and be-
 626 low the threshold of motion. Thus, we obtain

$$\theta = (35.4 \pm 2.3) \sqrt{C_d} \frac{14\tau_*^{2.5}}{1 + (\tau_{*c}/\tau_*)^4}. \quad (27)$$

627 Lastly, we consider $C_d = f(Re_p)$ after Ferguson and Church (2004).

628 Equation (27) was used to estimate θ for available observations of planar topog-
 629 raphy, bedload sheets, ripples, and dunes plotted in Figure 1. Results are plotted in Fig-
 630 ure 7. This exercise reveals that there is a range of θ values where both planar topog-
 631 raphy and bedforms are observed. However, estimated values of θ span almost seven or-
 632 ders of magnitude. Planar topography is almost exclusively observed when $\theta < 0.1$ and
 633 bedforms are exclusively observed when $\theta > 10$. Within this range, there is a strong
 634 trend in the relative frequencies with which different configurations are observed with
 635 increasing θ . Critically, planar topography is more commonly observed when $\theta < 1$, while
 636 bedforms are more commonly observed when $\theta > 1$.

637 Figure 8 shows the stability field for planar topography implied by (27). To illus-
 638 trate that our results are not sensitive to the choice of empirical bedload transport for-
 639 mula, the threshold of bedform initiation predicted using the (Wong & Parker, 2006) bed-
 640 load equation is also plotted. Nonzero values of ε lead to a slightly different form for (27)
 641 because θ has an additional dependence on $[0.75C_d(\tau_* - \tau_{*c})]^{5/2}$. However, this effect
 642 essentially shifts isocontours of θ up or down while preserving the overall qualitative trends.
 643 We emphasize that this model is derived assuming that bedform initiation occurs un-

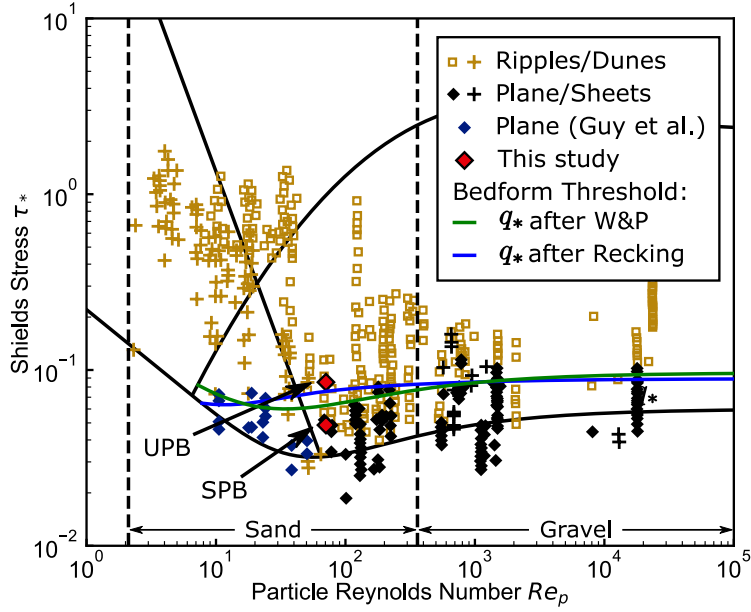


Figure 8. Shields-Parker river sedimentation diagram with theoretical plane bed/bedform transition obtained by solving equation 27 for $\theta = 1$ using two different bedload equations (Wong & Parker, 2006; Recking, 2013). Observations of planar topography and bedload sheets reported by Carling (1999) are plotted for comparison. Also plotted are observations of planar topography reported by Guy et al. (1966) that were ignored by Southard and Boguchwal (1990) and van den Berg and van Gelder (1993) in delineating classic stability fields.

644
645
646
647

der bedload-dominated transport conditions. This assumption is critical, both for the collision model described in section 2, and to scale the flux in equation (26). The stability field for lower-stage plane bed implied by (27) is not plotted above the threshold of significant suspension in Figure 8 for this reason.

648
649
650
651
652
653
654
655

Observations reported by Carling (1999) are plotted in Figure 8 for comparison with theory. This figure also includes observations of planar topography reported by Guy et al. (1966) that were ignored in subsequent studies because they are within the hydraulically smooth regime. Southard and Boguchwal (1990) asserted that these conditions would have eventually produced ripples; however, we suggest that planar topography may actually be stable indefinitely. Overall, the proposed stability field for lower-stage plane bed topography mirrors the empirical stability fields delineated using this observational data (Figure 1) but extends into the hydraulically smooth regime.

656
657
658
659
660
661
662

Experiments described in section 3 are also plotted in Figure 8. Note that the estimate of the stress τ_* depends on the same empirical formulae used to compute the critical value of the excess stress corresponding to $\theta = 1$. As a result, any error in the estimated value of τ_* will correspond to a commensurate error in the critical stress for bedform initiation. Uncertainty is not plotted in Figure 8 because we believe Figure 6 provides the most appropriate representation of uncertainty in experimental conditions relative to the predicted threshold of bedform initiation.

663
664
665
666

An outcome of this exercise is that the transition from rarefied to collisional transport predicted from (27) is similar to the to the transport thresholds described by other authors. For example, Pfeiffer and Finnegan (2018) describe a transition from marginal to full mobility that occurs at approximately twice the critical stress for sediment mo-

667 tion. Other authors have identified an important transition from intermittent to contin-
 668 uous transport (e.g., González et al., 2017; Pähtz et al., 2020) that is characterized by
 669 a profound reduction in the variability in the total momentum of particles over a finite
 670 bed area that also occurs at roughly twice the critical stress for sediment motion. We
 671 suggest that the alignment of these thresholds supports our use of kinetic theory for defin-
 672 ing a critical transport rate.

673 4.1 Discussion

674 In the preceding sections, we presented two proof-of-concept tests to evaluate whether
 675 the transition from stable to unstable planar topography near the threshold of motion
 676 can be explained by a transition from rarefied to collisional transport conditions as rep-
 677 resented in the dimensionless parameter θ . The first test (section 3) involves direct mea-
 678 surements of particle motion over stable and unstable planar topography, and reveals
 679 that θ increases by nearly a factor of ten, $\theta = 0.14$ to $\theta = 1.33$. The second test (sec-
 680 tion 4) involves estimating θ for observations of planar topography and bedforms across
 681 a wide range of conditions. Despite significant uncertainty in the value of θ in observa-
 682 tional data, we find that there is a shift in the most commonly observed bed configura-
 683 tion at $\theta = 1$.

684 The dimensionless parameter θ may be interpreted as a collision number scaling
 685 the average number of particle collisions per hop, or as an inverse Knudsen number quan-
 686 tifying the degree of granular rarefaction at the scale of individual particle motions. We
 687 argue that these interpretations serve to unify two parallel research paradigms in bed-
 688 form science. The first paradigm is focused on observation, documentation, and inter-
 689 pretation of phenomena and has led to conceptual models of bedform initiation that em-
 690 phasize the importance of particle collisions (e.g., Coleman & Nikora, 2009). In this view,
 691 planar topography is unstable when $\theta > 1$ because particle collisions become frequent
 692 enough to shift the balance between bed disturbance growth and relaxation. In other
 693 words, when sediment transport is rarefied at the scale of individual particle motions,
 694 bed disturbance greater than one particle diameter above or below the mean bed ele-
 695 vation are rapidly eroded or filled in, and collisions are needed to build larger, stabilized
 696 disturbances. The second paradigm focuses on mathematical analysis of perturbations
 697 subject to the coupled equations for flow, sediment transport, and topography (e.g., Char-
 698 rou et al., 2013). This approach generally predicts that planar topography is unstable un-
 699 der weak bedload transport conditions in rivers and involves continuum descriptions of
 700 sediment transport that are only valid if the mean free path is much smaller than the
 701 lengthscale of important fluctuations. In this view, we suggest that planar topography
 702 is stable when $\theta < 1$ because the expected instability is overwhelmed by effects asso-
 703 ciated with grain-scale fluctuations in transport rate. We argue that these two interpre-
 704 tations provide compatible descriptions of bedform initiation.

705 We recognize that neither of the tests presented here provide unequivocal proof that
 706 our hypothesis is correct; building a scientific consensus would require much more data
 707 than is available at this time. Instead, we suggest that the most convincing support comes
 708 from the overall compatibility with multiple disparate lines of evidence including mea-
 709 surements of particle motion and observations of bed configuration reported by other au-
 710 thors. In particular, we emphasize that our hypothesis is consistent with a long tradi-
 711 tion of descriptive studies that evince the importance of particle collisions while provid-
 712 ing a link to linear stability theory.

713 Our work leads to several new questions. First, do correlations in particle activ-
 714 ity and velocity influence the stable bed configuration? Our hypothesis depends on a heuris-
 715 tic analogy to kinetic gas theory because it is currently not clear how correlations in bed-
 716 load transport influence the mean free path and collision frequency. While we argue that
 717 this approach provides a reasonable estimate of θ , it is likely that the importance of cor-

relations varies in different settings and may play a role in governing the stable bed configuration. We note that the collision frequency for particles in a turbulent flow depends on a Stokes number quantifying the extent to which particle motions follow fluid motions. When particles perfectly follow the fluid, the collision frequency depends on the turbulent shear rate rather than the particle velocity (Saffman & Turner, 1956). Several studies have proposed models for collision frequency at intermediate Stokes numbers common in rivers (J. J. E. Williams & Crane, 1983; Sommerfeld, 2001; Oesterle & Petitjean, 1993), but these do not account for collisions with the bed that are important to bedload particle motions. Future advances in bedload particle kinetics may clarify these issues.

Another important question is why the transition from planar topography to bedforms captured in Figure 7 is gradual rather than abrupt. Overlapping observations may simply reflect the substantial uncertainties associated with empirical bedload transport formulae used to predict θ , or they may be a genuine feature of the data. Some authors have described planar beds that remain stable indefinitely unless an artificial defect is introduced (Southard & Dingler, 1971; Costello, 1974), indicating that planar topography and bedforms are metastable for a narrow range of conditions and the observed configuration. In this case, the observed condition depends on other factors like conditions at the flume and outlet or the history of the bed. If both configurations are stable for some conditions, the systematic trend in the relative frequency of observed bed configurations (Figure 7) suggests that the propensity for bedform initiation increases with θ . Alternatively, the stable bed configuration may be controlled by a third parameter that is not uniquely constrained by τ_* and Re_p . Possible candidates include the slope, Froude number, the relative particle submergence, or the particle Stokes number (which, we note, are not independent). The Stokes number in particular may be important for the reasons outlined above. The slope may also be important as it influences the value of τ_{*c} relative to that predicted by Brownlie (1981).

5 Conclusions

This paper investigates grain-scale transport processes at the onset of ripple and dune initiation. As a starting point, we recognize that the concept of planar topography breaks down at the granular scale and propose a definition of lower-stage plane bed topography that encompasses microforms with amplitudes that scale with particle diameter. This definition is appropriate because it is aligned with a hypothesized transition in the processes governing the relief of the bed. It is also aligned with practical considerations related to form roughness, drag partitioning, and preserved sedimentary structures.

Previous studies suggest that particle collisions are important during the initial phase of bedform development. We hypothesize that quasi-planar topography becomes unstable due to a critical transition in particle behavior that is related to particle collisions and propose a dimensionless parameter θ to quantify this transition. We show that θ is also an inverse Knudsen number that quantifies whether continuum models are permissible at an elementary morphodynamic lengthscale (the mean particle hop distance). Thus, an equivalent hypothesis is that planar topography is unstable when the expected morphodynamic instability is overwhelmed by granular effects.

We present two tests to evaluate whether our hypothesis is compatible with observations. First, we estimate the collision number from experimental measurements of tracer particle motion over stable and unstable planar topography. We find that the collision number is 0.14 in the stable plane bed experiment and 1.33 in the unstable plane bed experiment. Second, we incorporate empirical models for particle motion to estimate the collision numbers for an extensive database of observations bed configuration. While there is significant overlap in the observed bed configuration as a function of θ , we find that

769 (a) the relative frequency of observations exhibits a systematic trend as a function of θ
 770 with a shift in the most commonly observed configuration at $\theta = 1$, and (b) the con-
 771 dition where $\theta = 1$ mirrors classic empirical stability diagrams. These findings support
 772 the notion that particle collisions drive a shift in the balance between granular distur-
 773 bance growth and relaxation and suggest that lower-stage plane bed topography is an
 774 outcome of rarefied, intermittent sediment transport.

775 Acknowledgments

776 We thank the donors of the American Chemical Society Petroleum Research Fund 54492-
 777 DNI8, the National Science Foundation (NSF) grant EAR-1632938, and the University
 778 of Wyoming School of Energy Resources for partially supporting this research. We also
 779 thank Jelle ten Harkel, Noortje Oosterhoff, and Avelon Gerritsma for assistance with ex-
 780 periments and particle tracking. We thank Thomas Pätz, Stephane Bertin, two anony-
 781 mous reviewers, Associate Editor Christophe Ancey, and Editor Amy East for insight-
 782 ful critical feedback that improved the paper. Data and code are available through Figshare
 783 (Ashley, Naqshband, & McElroy, 2020).

784 References

- 785 Abramian, A., Devauchelle, O., Seizilles, G., & Lajeunesse, E. (2019). Boltzmann
 786 distribution of sediment transport. *Physical Review Letters*, *123*(1). doi: 10
 787 .1103/PhysRevLett.123.014501
- 788 Ancey, C. (2010). Stochastic modeling in sediment dynamics: Exner equation for
 789 planar bed incipient bed load transport conditions. *Journal of Geophysical Re-
 790 search: Earth Surface*, *115*(F2), 1–21. doi: 10.1029/2009JF001260
- 791 Ancey, C., Davison, A. C., Böhm, T., Jodeau, M., & Frey, P. (2008). Entrainment
 792 and motion of coarse particles in a shallow water stream down a steep slope.
 793 *Journal of Fluid Mechanics*, *595*, 83–114. doi: 10.1017/S0022112007008774
- 794 Ancey, C., & Heyman, J. (2014). A microstructural approach to bed load transport:
 795 mean behaviour and fluctuations of particle transport rates. *Journal of Fluid
 796 Mechanics*, *744*, 129–168. doi: 10.1017/jfm.2014.74
- 797 Andreotti, B., Claudin, P., & Douady, S. (2002). Selection of dune shapes and ve-
 798 locities part 2: A two-dimensional modelling. *European Physical Journal B*,
 799 *28*(3), 341–352. doi: 10.1140/epjb/e2002-00237-3
- 800 Andreotti, B., Claudin, P., & Pouliquen, O. (2010). Measurements of the aeolian
 801 sand transport saturation length. *Geomorphology*, *123*(3-4), 343–348. doi: 10
 802 .1016/j.geomorph.2010.08.002
- 803 Ashley, T. C., Mahon, R. C., Naqshband, S., Leary, K. C. P., & McElroy, B. (2020).
 804 Probability distributions of particle hop distance and travel time over equi-
 805 librium mobile bedforms. *Journal of Geophysical Research: Earth Surface*,
 806 *125*(7). doi: 10.1029/2020JF005647
- 807 Ashley, T. C., Naqshband, S., & McElroy, B. J. (2020). Data and code for "Par-
 808 ticle collisions control stable bed configuration under weak bedload transport
 809 conditions". *Figshare Dataset*. doi: 10.6084/m9.figshare.12475865.v2
- 810 Aussillous, P., Chauchat, J., Pailha, M., Médale, M., & Guazzelli, É. (2013). Inves-
 811 tigation of the mobile granular layer in bedload transport by laminar shearing
 812 flows. *Journal of Fluid Mechanics*, *736*, 594–615. doi: 10.1017/jfm.2013.546
- 813 Aussillous, P., Zou, Z., Guazzelli, É., Yan, L., & Wyart, M. (2016). Scale-free chan-
 814 neling patterns near the onset of erosion of sheared granular beds. *Proceedings
 815 of the National Academy of Sciences of the United States of America*, *113*(42),
 816 11788–11793. doi: 10.1073/pnas.1609023113
- 817 Baas, J. H., Best, J. L., & Peakall, J. (2016). Predicting bedforms and primary cur-
 818 rent stratification in cohesive mixtures of mud and sand. *Journal of the Geo-
 819 logical Society*, *173*(1), 12–45. doi: 10.1144/jgs2015-024

- 820 Bagnold, R. A. (1935). The movement of desert sand. *Proceedings of the Royal*
821 *Society of London. Series A - Mathematical and Physical Sciences*, 157(892),
822 594–620. doi: 10.1098/rspa.1936.0218
- 823 Ballio, F., Pokrajac, D., Radice, A., & Hosseini Sadabadi, S. A. (2018). Lagrangian
824 and Eulerian description of bed load transport. *Journal of Geophysical Re-*
825 *search: Earth Surface*, 123(2), 384–408. doi: 10.1002/2016JF004087
- 826 Best, J. L. (1992). On the entrainment of sediment and initiation of bed defects: in-
827 sights from recent developments within turbulent boundary layer research. *Sed-*
828 *imentology*, 39(5), 797–811. doi: 10.1111/j.1365-3091.1992.tb02154.x
- 829 Best, J. L. (1996). The fluid dynamics of small-scale alluvial bedforms. In P. A. Car-
830 ling & M. R. Dawson (Eds.), *Advances in fluvial dynamics and stratigraphy*
831 (pp. 67–125). Manchester, United Kingdom: John Wiley and Sons.
- 832 Best, J. L. (2005). The fluid dynamics of river dunes: A review and some future
833 research directions. *Journal of Geophysical Research: Earth Surface*, 110(F4).
834 doi: 10.1029/2004JF000218
- 835 Bohorquez, P., Cañada-Pereira, P., Jimenez-Ruiz, P. J., & del Moral-Erencia,
836 J. D. (2019). The fascination of a shallow-water theory for the formation
837 of megaflood-scale dunes and antidunes. *Earth-Science Reviews*, 193(April),
838 91–108. doi: 10.1016/j.earscirev.2019.03.021
- 839 Bradski, G. (2000). The OpenCV library. *Dr. Dobb's Journal of Software Tools*, 25.
- 840 Brownlie, W. R. (1981). *Prediction of flow depth and sediment discharge in open*
841 *channels* (Tech. Rep. No. 43A). Pasadena, California: W. M. Keck Laboratory
842 of Hydraulics and Water Resources, California Institute of Technology.
- 843 Carling, P. A. (1999). Subaqueous gravel dunes. *Journal of Sedimentary Research*,
844 69(3), 534–545. doi: 10.2110/jsr.69.534
- 845 Charru, F., Andreotti, B., & Claudin, P. (2013). Sand ripples and dunes. *Annual*
846 *Review of Fluid Mechanics*, 45(1), 469–493. doi: 10.1146/annurev-fluid-011212
847 -140806
- 848 Chaudhry, M. H. (1993). *Open-Channel Flow*. Englewood Cliffs: Prentice-Hall.
- 849 Christensen, R., Johnson, W., Branscum, A., & Hanson, T. E. (2011). Simulations.
850 In *Bayesian ideas data analysis: An introduction for scientists and statisticians*
851 (chap. 6). Boca Raton, FL: CRC Press.
- 852 Clifford, N. J., Robert, A., & Richards, K. S. (1992). Estimation of flow resistance
853 in gravel-bedded rivers: A physical explanation of the multiplier of rough-
854 ness length. *Earth Surface Processes and Landforms*, 17(2), 111–126. doi:
855 10.1002/esp.3290170202
- 856 Coleman, S. E., & Melville, B. W. (1994). Bed-form development. *Journal of*
857 *Hydraulic Engineering*, 120(5), 544–560. doi: 10.1061/(ASCE)0733-9429(1994)
858 120:5(544)
- 859 Coleman, S. E., & Melville, B. W. (1996). Initiation of bed forms on a flat sand
860 bed. *Journal of Hydraulic Engineering*, 122(6), 301–309. doi: 10.1061/(asce)
861 0733-9429(1996)122:6(301)
- 862 Coleman, S. E., & Nikora, V. I. (2009). Bed and flow dynamics leading to
863 sediment-wave initiation. *Water Resources Research*, 45(4), 1–12. doi:
864 10.1029/2007WR006741
- 865 Coleman, S. E., & Nikora, V. I. (2011). Fluvial dunes: Initiation, characterization,
866 flow structure. *Earth Surface Processes and Landforms*, 36(1), 39–57. doi: 10
867 .1002/esp.2096
- 868 Costello, W. R. (1974). *Development of bed configurations in coarse sands* (Ph.D.
869 Dissertation). Massachusetts Institute of Technology.
- 870 Costello, W. R., & Southard, J. B. (1981). Flume experiments on lower-flow-regime
871 bed forms in coarse sand. *SEPM Journal of Sedimentary Research*, 51(3), 849–
872 864. doi: 10.1306/212F7DC4-2B24-11D7-8648000102C1865D
- 873 Dade, W. B., & Friend, P. F. (1998). Grain size, sediment-transport regime and
874 channel slope in alluvial rivers. *Journal of Geology*, 106(6), 661–675.

- 875 Dunne, K. B., & Jerolmack, D. J. (2018). Evidence of, and a proposed explanation for, bimodal transport states in alluvial rivers. *Earth Surface Dynamics*,
876 6, 583–594. doi: 10.5194/esurf-6-583-2018
- 878 Eaton, B. C., Church, M., & Millar, R. G. (2004). Rational regime model of al-
879 luvial channel morphology and response. *Earth Surface Processes and Land-*
880 *forms*, 29(4), 511–529. doi: 10.1002/esp.1062
- 881 Einstein, H. A. (1950). The bed-load function for sediment transportation in open
882 channel flows. *U.S. Department of Agriculture Technical Bulletin 1026*.
- 883 Engelund, F., & Fredsoe, J. (1982). Sediment ripples and dunes. *Annual Review of*
884 *Fluid Mechanics*, 14(1), 13–37. doi: 10.1146/annurev.fl.14.010182.000305
- 885 Engelund, F., & Hansen, E. (1967). *A monograph on sediment transport in alluvial*
886 *streams* (Tech. Rep.). Technical University of Denmark. doi: 10.1007/s13398
887 -014-0173-7.2
- 888 Fathel, S., Furbish, D. J., & Schmeeckle, M. W. (2015). Experimental evidence
889 of statistical ensemble behavior in bed load sediment transport. *Jour-*
890 *nal of Geophysical Research: Earth Surface*, 120(11), 2298–2317. doi:
891 10.1002/2015JF003552
- 892 Ferguson, R. I., & Church, M. (2004). A simple universal equation for grain set-
893 tling velocity. *Journal of Sedimentary Research*, 74(6), 933–937. doi: 10.1306/
894 051204740933
- 895 Fourrière, A., Claudin, P., & Andreotti, B. (2010). Bedforms in a turbulent stream:
896 Formation of ripples by primary linear instability and of dunes by nonlin-
897 ear pattern coarsening. *Journal of Fluid Mechanics*, 649, 287–328. doi:
898 10.1017/S0022112009993466
- 899 Fredsoe, J. (1982). Shape and dimensions of stationary dunes in rivers. *Journal of*
900 *the Hydraulics Division of the American Society of Civil Engineers*, 108(8),
901 932–947.
- 902 Furbish, D. J. (1997). *Fluid physics in geology: An introduction to fluid motions on*
903 *Earth's surface and within its crust*. New York: Oxford University Press.
- 904 Furbish, D. J., Ball, A. E., & Schmeeckle, M. W. (2012). A probabilistic de-
905 scription of the bed load sediment flux: 4. Fickian diffusion at low trans-
906 port rates. *Journal of Geophysical Research: Earth Surface*, 117(F3). doi:
907 10.1029/2012JF002356
- 908 Furbish, D. J., Fathel, S. L., Schmeeckle, M. W., Jerolmack, D. J., & Schumer,
909 R. (2017). The elements and richness of particle diffusion during sediment
910 transport at small timescales. *Earth Surface Processes and Landforms*, 42(1),
911 214–237. doi: 10.1002/esp.4084
- 912 Furbish, D. J., Haff, P. K., Roseberry, J. C., & Schmeeckle, M. W. (2012). A prob-
913 abilistic description of the bed load sediment flux: 1. Theory. *Journal of Geo-*
914 *physical Research: Earth Surface*, 117(F3). doi: 10.1029/2012JF002352
- 915 Furbish, D. J., & Schmeeckle, M. W. (2013). A probabilistic derivation of the
916 exponential-like distribution of bed load particle velocities. *Water Resources*
917 *Research*, 49(3), 1537–1551. doi: 10.1002/wrcr.20074
- 918 Furbish, D. J., Schmeeckle, M. W., Schumer, R., & Fathel, S. L. (2016). Prob-
919 ability distributions of bed load particle velocities, accelerations, hop dis-
920 tances, and travel times informed by Jaynes's principle of maximum entropy.
921 *Journal of Geophysical Research: Earth Surface*, 121(7), 1373–1390. doi:
922 10.1002/2016JF003833
- 923 García, M. H. (2008). Sediment transport and morphodynamics. In *Sedimen-*
924 *tation engineering* (pp. 21–163). Reston, VA: American Society of Civil Engi-
925 neers. doi: 10.1061/9780784408148.ch02
- 926 González, C., Richter, D. H., Bolster, D., Bateman, S., Calantoni, J., & Escauriaza,
927 C. (2017). Characterization of bedload intermittency near the threshold of
928 motion using a Lagrangian sediment transport model. *Environmental Fluid*
929 *Mechanics*, 17(1), 111–137. doi: 10.1007/s10652-016-9476-x

- 930 Guy, H., Simons, D. B., & Richardson, E. (1966). Summary of alluvial channel data
931 from flume experiments, 1956-61. *U.S. Geology Survey Professional Paper 462-*
932 *I*.
- 933 Gyr, A., & Kinzelbach, W. (2004). Bed forms in turbulent channel flow. *Applied Me-*
934 *chanics Reviews*, 57(1), 77–93. doi: 10.1115/1.1584063
- 935 Gyr, A., & Schmid, A. (1989). The different ripple formation mechanisms. *Journal*
936 *of Hydraulic Research*, 27(1), 61–74. doi: 10.1080/00221688909499244
- 937 Heyman, J., Ma, H. B., Mettra, F., & Ancey, C. (2014). Spatial correlations in bed
938 load transport: Evidence, importance, and modeling. *Journal of Geophysical*
939 *Research F: Earth Surface*, 119(8), 1751–1767. doi: 10.1002/2013JF003003
- 940 Houssais, M., Ortiz, C. P., Durian, D. J., & Jerolmack, D. J. (2016). Rheology of
941 sediment transported by a laminar flow. *Physical Review E*, 94(6), 1–10. doi:
942 10.1103/PhysRevE.94.062609
- 943 Ikeda, S., Parker, G., & Kimura, Y. (1988). Stable width and depth of straight
944 gravel rivers with heterogeneous bed materials. *Water Resources Research*,
945 24(5), 713–722. doi: 10.1029/WR024i005p00713
- 946 Kauzmann, W. (2012). *Kinetic theory of gases* (2nd ed.). Mineola, New York: Dover
947 Publications, Inc.
- 948 Lacey, G. (1930). Stable channels in alluvium. *Minutes of the Proceedings of*
949 *the Institution of Civil Engineers, Thomas Telford-ICE Virtual Library*, 229,
950 259–292.
- 951 Lajeunesse, E., Malverti, L., & Charru, F. (2010). Bed load transport in turbulent
952 flow at the grain scale: Experiments and modeling. *Journal of Geophysical Re-*
953 *search: Earth Surface*, 115(4). doi: 10.1029/2009JF001628
- 954 Langbein, W. B., & Leopold, L. B. (1968). River channel bars and dunes - Theory
955 of kinematic waves. *U.S. Geological Survey Professional Paper 422-L*.
- 956 Leary, K. C. P., & Ganti, V. (2020). Preserved fluvial cross strata record bedform
957 disequilibrium dynamics. *Geophysical Research Letters*, 47(2). doi: 10.1029/
958 2019GL085910
- 959 Leary, K. C. P., & Schmeeckle, M. W. (2017). The importance of splat events to
960 the spatiotemporal structure of near-bed fluid velocity and bedload motion
961 over bedforms: Laboratory experiments downstream of a backward-facing step.
962 *Journal of Geophysical Research: Earth Surface*. doi: 10.1002/2016JF004072
- 963 Leclair, S. F., & Bridge, J. S. (2001). Quantitative interpretation of sedimentary
964 structures formed by river dunes. *SEPM Journal of Sedimentary Research*,
965 71(2), 713–716. doi: 10.1306/D4268D79-2B26-11D7-8648000102C1865D
- 966 Leeder, M. R. (1980). Discussion of the stability of lower stage plane beds and the
967 absence of current ripples in coarse sands. *Journal of the Geological Society*,
968 138(6), 753–754. doi: 10.1144/gsjgs.138.6.0753
- 969 Liu, M. X., Pelosi, A., & Guala, M. (2019). A statistical description of particle mo-
970 tion and rest regimes in open-channel flows under low bedload transport. *Jour-*
971 *nal of Geophysical Research: Earth Surface*, 124(11), 2666–2688. doi: 10.1029/
972 2019JF005140
- 973 Mahon, R. C., & McElroy, B. (2018). Indirect estimation of bedload flux from mod-
974 ern sand-bed rivers and ancient fluvial strata. *Geology*, 46(7), 579–582. doi: 10
975 .1130/G40161.1
- 976 Martin, R. L., & Kok, J. F. (2018). Distinct Thresholds for the Initiation and Ces-
977 sation of Aeolian Saltation From Field Measurements. *Journal of Geophysical*
978 *Research: Earth Surface*, 123(7), 1546–1565. doi: 10.1029/2017JF004416
- 979 Martin, R. L., Purohit, P. K., & Jerolmack, D. J. (2014). Sedimentary bed evolution
980 as a mean-reverting random walk: Implications for tracer statistics. *Geophys-*
981 *ical Research Letters*, 41, 6152–6159. doi: 10.1002/2014GL060525
- 982 McLean, S. R. (1990). The stability of ripples and dunes. *Earth-Science Reviews*,
983 29(1-4), 131–144. doi: 10.1016/0012-8252(0)90032-Q
- 984 Métivier, F., Lajeunesse, E., & Devauchelle, O. (2017). Laboratory rivers: Lacey’s

- law, threshold theory, and channel stability. *Earth Surface Dynamics*, 5, 187–198. doi: 10.5194/esurf-5-187-2017
- Naqshband, S., McElroy, B., & Mahon, R. C. (2017). Validating a universal model of particle transport lengths with laboratory measurements of suspended grain motions. *Water Resources Research*, 53(5), 4106–4123. doi: 10.1002/2016WR020024
- Oesterle, B., & Petitjean, A. (1993). Simulation of particle-to-particle interactions in gas solid flows. *International Journal of Multiphase Flow*, 19(1), 199–211. doi: 10.1016/0301-9322(93)90033-Q
- Pähtz, T., Clark, A. H., Valyrakis, M., & Durán, O. (2020). The physics of sediment transport initiation, cessation, and entrainment across aeolian and fluvial environments. *Reviews of Geophysics*, 58(1). doi: 10.1029/2019RG000679
- Paola, C., & Borgman, L. (1991). Reconstructing random topography from preserved stratification. *Sedimentology*, 38(4), 553–565. doi: 10.1111/j.1365-3091.1991.tb01008.x
- Parker, G., & Wilcock, P. (1993). Sediment Feed and Recirculating Flumes: Fundamental Difference. *Journal of Hydraulic Engineering*, 119(11), 1192–1204.
- Parker, G., Wilcock, P. R., Paola, C., Dietrich, W. E., & Pitlick, J. (2007). Physical basis for quasi-universal relations describing bankfull hydraulic geometry of single-thread gravel bed rivers. *Journal of Geophysical Research*, 112(F4), F04005. doi: 10.1029/2006JF000549
- Pfeiffer, A. M., & Finnegan, N. J. (2018). Regional Variation in Gravel Riverbed Mobility, Controlled by Hydrologic Regime and Sediment Supply. *Geophysical Research Letters*, 45(7), 3097–3106. doi: 10.1002/2017GL076747
- Rapp, B. E. (2017). Fluids. In *Microfluidics: Modelling, mechanics and mathematics* (pp. 243–263). Oxford, UK: Elsevier. doi: 10.1016/B978-1-4557-3141-1.50009-5
- Raudkivi, A. J. (1963). Study of sediment ripple formation. *Journal of the Hydraulic Division of the American Society of Civil Engineers*, 89(6), 15–34.
- Raudkivi, A. J. (1966). Bed forms in alluvial channels. *Journal of Fluid Mechanics*, 26(3), 507–514. doi: 10.1017/S0022112066001356
- Recking, A. (2013). Simple Method for Calculating Reach-Averaged Bed-Load Transport. *Journal of Hydraulic Engineering*, 139(1), 70–75. doi: 10.1061/(asce)hy.1943-7900.0000653
- Saffman, P. G., & Turner, J. S. (1956). On the collision of drops in turbulent clouds. *Journal of Fluid Mechanics*, 1(1), 16–30. doi: 10.1017/S0022112056000020
- Schindelin, J., Arganda-Carreras, I., Frise, E., Kaynig, V., Longair, M., Pietzsch, T., ... Cardona, A. (2012). Fiji: an open-source platform for biological-image analysis. *Nature Methods*, 9(7), 676–682. doi: 10.1038/nmeth.2019
- Schumm, S. (1960). The shape of alluvial channels in relation to sediment type. *U.S. Geological Survey Professional Paper 352-B*.
- Smith, J. D., & Mclean, S. R. (1977). Spatially averaged flow over a wavy surface. *Journal of Geophysical Research*, 82(20). doi: 10.1029/JC082i012p01735
- Sommerfeld, M. (2001). Validation of a stochastic Lagrangian modelling approach for inter-particle collisions in homogeneous isotropic turbulence. *International Journal of Multiphase Flow*, 27(10), 1829–1858. doi: 10.1016/S0301-9322(01)00035-0
- Southard, J. B., & Boguchwal, L. A. (1990). Bed configurations in steady unidirectional water flows. Part 2. Synthesis of flume data. *Journal of Sedimentary Petrology*, 60(5), 658–679. doi: 10.1306/212f9241-2b24-11d7-8648000102c1865d
- Southard, J. B., & Dingler, J. R. (1971). Flume study of ripple propagation behind mounds on flat sand beds. *Sedimentology*, 16, 251–263. doi: 10.1111/j.1365-3091.1971.tb00230.x
- Tinevez, J., Perry, N., Schindelin, J., Hoopes, G. M., Reynolds, G. D., Laplan-

- 1040 tine, E., . . . Eliceiri, K. W. (2017). TrackMate: An open and exten-
 1041 sible platform for single-particle tracking. *Methods*, *115*, 80–90. doi:
 1042 10.1016/j.ymeth.2016.09.016
- 1043 van den Berg, J. H., & van Gelder, A. (1993). A new bedform stability diagram,
 1044 with emphasis on the transition of ripples to plane bed in flows over fine sand
 1045 and silt. In *Alluvial sedimentation* (pp. 11–21). Oxford, UK: Blackwell Pub-
 1046 lishing Ltd. doi: 10.1002/9781444303995.ch2
- 1047 van Rijn, L. (1984). Sediment transport, part III: Bed forms and alluvial roughness.
 1048 *Journal of Hydraulic Engineering*, *110*(12), 1733–1755.
- 1049 Venditti, J. G., Church, M., & Bennett, S. J. (2005b). On the transition between 2D
 1050 and 3D dunes. *Sedimentology*, *52*(6), 1343–1359. doi: 10.1111/j.1365-3091.2005
 1051 .00748.x
- 1052 Venditti, J. G., Church, M. A., & Bennett, S. J. (2005a). Bed form initiation from
 1053 a flat sand bed. *Journal of Geophysical Research: Earth Surface*, *110*(1), 1–19.
 1054 doi: 10.1029/2004JF000149
- 1055 Whiting, P. J., & Dietrich, W. E. (1990). Boundary shear stress and roughness over
 1056 mobile alluvial beds. *Journal of Hydraulic Engineering*, *116*(12), 1495–1511.
 1057 doi: 10.1061/(ASCE)0733-9429(1990)116:12(1495)
- 1058 Wiberg, P. L., & Smith, J. D. (1989). Model for calculating bed load transport of
 1059 sediment. *Journal of Hydraulic Engineering*, *115*(1), 101–123. doi: 10.1061/
 1060 (ASCE)0733-9429(1989)115:1(101)
- 1061 Wilcock, P. R., & McArdeell, B. W. (1997). Partial transport of a sand/gravel sedi-
 1062 ment. *Water Resources Research*, *33*(1), 235–245. doi: 10.1029/96WR02672
- 1063 Wilkerson, G. V., & Parker, G. (2010). Physical basis for quasi-universal relation-
 1064 ships describing bankfull hydraulic geometry of sand-bed rivers. *Journal of*
 1065 *Hydraulic Engineering*, *137*(7), 739–753. doi: 10.1061/(ASCE)HY.1943-7900
 1066 .0000352
- 1067 Williams, J. J. E., & Crane, R. I. (1983). Particle collision rate in turbu-
 1068 lent flow. *International Journal of Multiphase Flow*, *9*(4), 421–435. doi:
 1069 10.1016/0301-9322(83)90098-8
- 1070 Williams, P. B., & Kemp, P. H. (1971). Initiation of ripples on flat sediment beds.
 1071 *Journal of the Hydraulic Division of the American Society of Civil Engineers*,
 1072 *97*(4), 502–522.
- 1073 Wong, M., & Parker, G. (2006). Reanalysis and correction of bed-load relation
 1074 of Meyer-Peter and Müller using their own database. *Journal of Hydraulic*
 1075 *Engineering*, *132*(11), 1159–1168. doi: 10.1061/(ASCE)0733-9429(2006)132:
 1076 11(1159)
- 1077 Wright, S. A., & Parker, G. (2004). Flow resistance and suspended load in sand-
 1078 bed rivers: Simplified stratification model. *Journal of Hydraulic Engineering*,
 1079 *130*(8), 796–805. doi: 10.1061/(ASCE)0733-9429(2004)130:8(796)